UNIVERSITY OF OSLO
Department of Geology

Fresnel Aperture Pre-Stack Depth Migration

Thomas Hellmann

12th January 2005

Contents

Acknowledgement

First, I would like to thank my supervisor, Pr. Leiv Jacob Gelius, for his guidance and patience during my *M.Sc.* thesis, but also for giving me the opportunity to work on this project, which allowed me to work both with the theory and the practice, through geophysics and programming. I consider this project as the perfect conclusion to all the years of my studies at the university.

I would also like to thank Dr. Hocine Tabti for his assistance, and CGG Norge for providing the field data I used for testing.

And I would like to express my gratitude to all the people who kicked my bottom and gave me the motivation necessary to continue through the bad moments: my supervisor Leiv Gelius, my flatmates Petri Lorenzo and Dorian Fructus, my family and especially my parents, and my collegues Evguenia Chelavina and Finn Foldal.

En god programmerer kan gjøre alt, så lenge det er i Fortran

Dorian Fructus (Teknisk Ukeblad, May 23rd 2003)

Chapter 1

Introduction

The Pre-Stack Depth Migration (PSDM) is one of the most important methods of seismic imaging. Compared to the similar method used in time-processing, its real advantage is to represent the underground structural geology with its actual geometry, in depth. This is of great interest while planning a drilling campaign or optimizing a production strategy, trying to get as much as possible out of the reservoir. More generally, it is the best method to image complex subsurface areas.

Therefore, improving its resolution is now a big issue. And try to get an accurate migration of the scattered energy recorded at the surface back to its real reflection position is a challenge.

New techniques, like the Wave Equation migration, give better results as soon as your target is located under a salt dome, or any volume with a strong impedance contrast that reduces the illumination of the target zone. But in most of the other cases, these methods cannot improve the resolution of an image, compared to the full aperture Kirchhoff pre-stack depth migration. And the Wave Equation migration is much more demanding in terms of computation ressources and time. Therefore, Pre-stack Kirchhoff Depth migration is still the most commonly used method.

In this thesis, I will present the results of a new approach to Pre-stack Kirchhoff Depth migration using the Kirchhoff algorithm and Fresnel aper-

ture features in order to improve the signal-to-noise ratio of the seismic data in depth imaging. Another advantage of this method is that it requires no additional measurements compared to the traditional PSDM. Indeed, the Fresnel apertures are picked interactively, in a way that is similar to velocity picking, and thereafter used during the migration process.

This method will, from now on, be refered to as *Fresnel Aperture Pre-stack Depth Migration* or FA-PSDM.

The main task during my study was to develop the tools needed to process the data using the FA-PSDM, once the ray tracing has been done. The tools were: a migration program and picking software to pick the Fresnel apertures. These will be presented in the fourth chapter. But first, the mathematical background will be introduced in the second chapter. The physical theories will follow, in the third chapter. At the end, the application of the FA-PSDM on both synthetic and field data will be presented and discussed in the fifth chapter.

The source code for the two programs are found in the appendix.

Chapter 2

Background

In this first chapter, I will introduce some important features that we will need later,in order to understand the postulats and limits of the Prestack Depth migration algorithm and its processing scheme. In this view, understanding the basics of Kirchhoff migration and ray tracing are essential. Furthermore, I will right away introduce some tools that I used to develop the new technique.

2.1 The Pre-Stack Depth migration basics

To help understand Pre-stack Depth Migration, let us present the core of this method: the Kirchhoff migration and the ray tracing.

2.1.1 The Kirchhoff migration

The goal of Prestack Depth Migration is to obtain the best image possible of the subsurface, by improved focusing and preservation of the high-frequencies in the dataset. I start here with Kirchhoff's representation of the reflected wave field at a given surface. Then, these equations will be derived for the special case of constant offset data and 2.5-D (cf. [6]). The 2.5-D approximation means that we use the 3-D point source model, but make the assumption that the geology is invariant laterally, in the off-line direction.

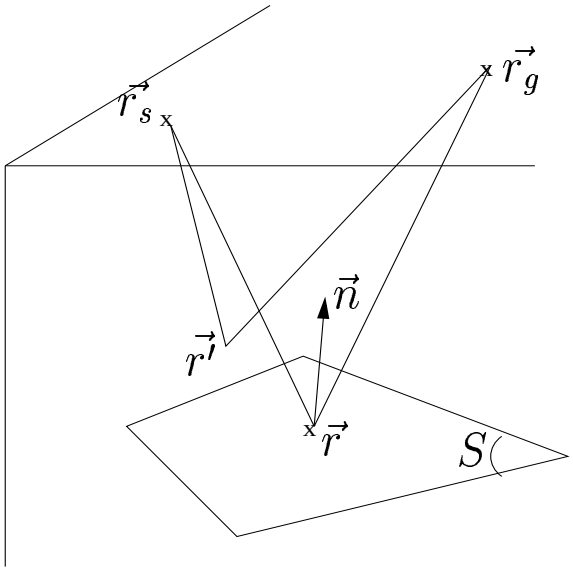

Figure 2.1: Geometry of the system used to develop the inversion operator in 2.5D.

First, we start from the wave equation, using the Helmholtz equation, which is valid for monochromatic waves:

$$\nabla^2 U_g(\omega, \vec{r}, \vec{r_s}) + (\frac{\omega}{v})^2 U_g = 0 \tag{2.1}$$

where U_g is the scattered field from the reflector, $\vec{r}$ a given point location and $\vec{r_s}$ the source location. Similarly, the receiver location will be called $\vec{r_g}$.

Let us now introduce the Green's function $g(\omega, \vec{r}, \vec{r_g})$ which describes the wave propagation from a point source at $\vec{r}$ to $\vec{r_g}$:

$$\nabla^2 g(\omega, \vec{r}, \vec{r_g}) + (\frac{\omega}{v})^2 g(\omega, \vec{r}, \vec{r_g}) = -\delta(\vec{r} - \vec{r_g}) \tag{2.2}$$

Expressing U_g as a function of g, and using the reciprocity of $\vec{r}$ and $\vec{r_g}$ (see Fig. 2.1), we get (cf [8]):

$$U_g(\omega, \vec{r_g}, \vec{r_s}) = \int\int dS[U_g(\omega, \vec{r}, \vec{r_s})\frac{\partial g(\omega, \vec{r}, \vec{r_g})}{\partial n} - g(\omega, \vec{r}, \vec{r_g})\frac{\partial U_g(\omega, \vec{r}, \vec{r_s})}{\partial n}] \tag{2.3}$$

where $\vec{n}$ is the normal vector to the reflector at $\vec{r}$, as shown in Fig. 2.1.

One of the solutions to Eq.(2.3) is:

$$g(\omega, \vec{r}, \vec{r_g}) = \frac{e^{\frac{i\omega}{v}|\vec{r_g} - \vec{r}|}}{4\pi|\vec{r_g} - \vec{r}|} \tag{2.4}$$

Consider now the high-frequency approximation, where $2\omega\frac{r}{v} >> 1$, r being the distance to the reflector, v the velocity and ω the frequency. Its normal derivative, using the high-frequencies approximation, can then be written as follow:

$$\frac{\partial g(\omega, \vec{r}, \vec{r_g})}{\partial n} \approx \frac{i\omega}{v}\nabla|\vec{r_g} - \vec{r}|\frac{\vec{n}}{n}\frac{e^{\frac{i\omega}{v}|\vec{r_g} - \vec{r}|}}{4\pi|\vec{r_g} - \vec{r}|} \tag{2.5}$$

Identically, we can write:

$$\frac{\partial U_g(\omega, \vec{r}, \vec{r_s})}{\partial n} \approx \frac{-i\omega}{v}\nabla|\vec{r} - \vec{r_s}|\frac{\vec{n}}{n}R\frac{e^{\frac{i\omega}{v}|\vec{r} - \vec{r_s}|}}{4\pi|\vec{r} - \vec{r_s}|} \tag{2.6}$$

where R is the angular dependent reflection coefficient.

We can now rewrite the expression of the scattered field:

$$U_g(\omega, \vec{r_g}, \vec{r_s}) \approx \frac{i\omega}{16\pi^2}\int\int dSR[\nu_s + \nu_g]\frac{e^{\frac{i\omega}{v}[|\vec{r} - \vec{r_s}| + |\vec{r_g} - \vec{r}|]}}{|\vec{r} - \vec{r_s}||\vec{r_g} - \vec{r}|} \tag{2.7}$$

where $\nu_{s/g} = \frac{\vec{r} - \vec{r_{s/g}}}{v|\vec{r} - \vec{r_{s/g}}|}\vec{n}$

This is the Kirchhoff wavefield response for offset modeling, if we employ the link to the midpoint-offset coordinates $\vec{y}$ and h as follows:

$\vec{y} = \frac{\vec{r_s} + \vec{r_g}}{2}$

$h = \frac{1}{2}\sqrt{(\vec{r_g} - \vec{r_s})(\vec{r_g} + \vec{r_s})}$

By moving the source/receiver configuration, the time section is constructed, each output trace given by a surface integration corresponding to the source/receiver geometry.

In the case of an inversion problem -and this the case here, an inversion operator is needed in order to determine the reflection interfaces within the model. Such an inversion scheme can be derived from use of Eq.(2.7). The idea is to find an inverse analogy to this equation through postulating that:

$$I =< R > \approx \int\int \eta U_g(\omega, \vec{r}_g, \vec{r}_s) d\vec{r}_g d\vec{r}_s \tag{2.8}$$

where I is an angle-averaged estimate of the reflection coefficient R and η is an inversion kernel. η can now be determined by combining Eqs.(2.7) and (2.8) and impose that every time the test data described by Eq.(2.7) are located on an interface a significant response should be obtained (cf. [10]).

First, we consider the case of 2.5-D, a single reflector and constant velocity. By 2.5-D, I mean that data are recorded along a single line, and that all parallel lines are considered as being identical to the original one. The reason for this assumption is that information about the lateral extent of the reflectors are needed so that a unique solution can be established for the inverse problem. We introduce a new variable, x, defining the axis along which the 2-D line is shot. Thus, the source position (x_s), the reflector point and the receiver position (x_g) are assumed to be functions of x only.

In the case of 2.5-D, the inversion formula can be expressed as follows (cf. [6]):

$$I(x,z) \simeq \int\int dx_s dx_g \int d\omega \sqrt{i\omega} W(x,z,x_s,x_g) e^{i\omega(t_s+t_g)} U_g(\omega, x_s, x_g) \tag{2.9}$$

where $W(x,z,x_s,x_g)$ is the weight applied to the data. We need this weight in order to control the migration amplitudes and avoid the migrated data to be contaminated by artifacts. t_s and t_g are, respectively, the traveltime from the source to the image point and from the image point to the receiver.

$\sqrt{i\omega}$ is a phase shift applied in the frequency domain which sharpens the pulse slightly. It is the 2.5-D counterpart to a time-differentiation in 3-D. Though, its omission does not alter the result significantly and it has not been taken into account in the program I used.

The weight factor W can be written explicitly as (cf. [7]):

$$W(x,z,x_s,x_g) = \frac{2z}{v^{\frac{3}{2}}\sqrt{\pi}}\sqrt{1+\frac{(x_s-x)(r_g-x)}{|x_s-x||x_g-x)|}}\sqrt{\frac{|x_s-x|+|x_g-x|}{|x_s-x||x_g-x|}}(\frac{|x_g-x|}{|x_s-x|}+\frac{|x_s-x|}{|x_g-x|}) \tag{2.10}$$

where (x,z) is the location of the image point.

Using simple geometrical principles and:

$x_{s/g} = vt_{s/g}$,

we can rewrite this equation as:

$$W = \sqrt{\frac{2}{\pi}}\frac{z}{v^2}(t_s+t_g)^{\frac{3}{2}}\sqrt{1-\frac{(x_s-x_g)^2}{v^2(t_s+t_g)^2}}(\frac{1}{t_s^2}+\frac{1}{t_g^2}) \tag{2.11}$$

Notice that t_s+t_g is the total traveltime and defines which sample of the trace that contributes to the formation of the output image point. x_s and x_g are here, respectively, the distance of the source and the receiver along the 2-D line from a chosen origin.

Up till now, I have discussed the case of a single reflector and a homogeneous overburden. The extension of Eqs.(2.9) and (2.10) to a general background case and several reflectors is straight forward. The velocity v will be space-variant, and the traveltimes t_s and t_g must be computed employing ray tracing methods, taking into account the velocity inhomogeneities.

2.1.2 The ray tracing

In this thesis, I used a ray tracing program based on the paraxial ray tracing technique (cf. [4]). This latter represents an efficient way of computing travel time tables used as input for the migration program.

The principle of ray tracing is to determine the Green's function between a source and a given receiver position. The process is then reiterated for all source and receiver points, one by one. But in the paraxial ray tracing method, the Green's functions are approximated away from the ray. In other words, it is not required to use dense two-point ray tracing, since one can

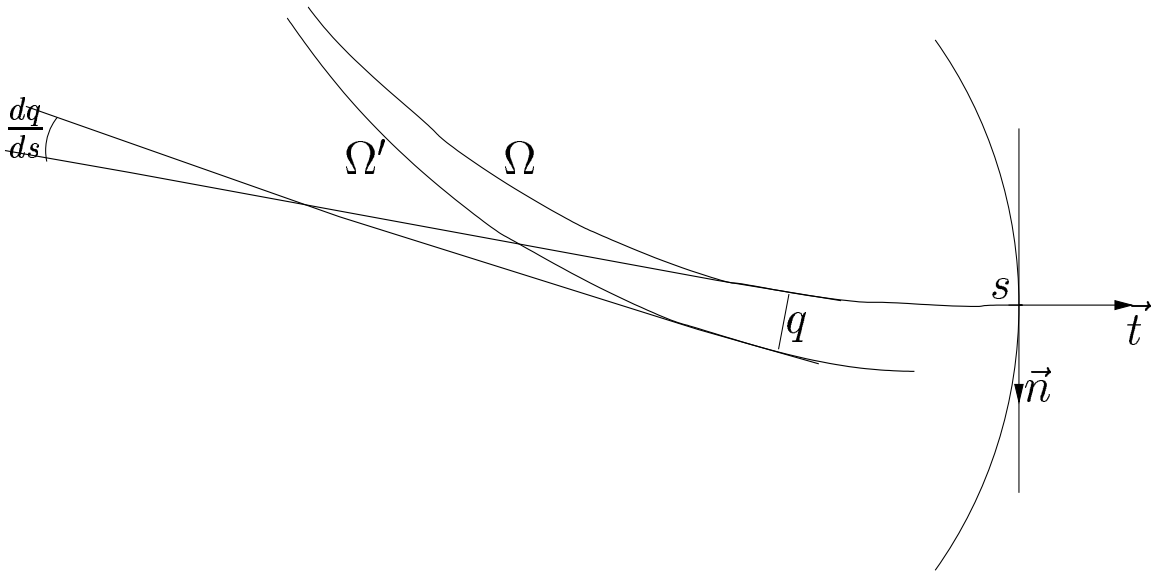

Figure 2.2: Geometrical illustration of the difference between a central ray (Ω) and a paraxial ray (Ω').

extrapolate the wave field in the vicinity of the receiver. That makes the ray tracing process less time-consuming.

The mathematical basis of this method is the one from the dynamic ray tracing. The equations involved relate changes in position and direction of a paraxial ray in the vincinity of the central ray to changes in that ray's initial conditions (cf. [2]).

Take the example of a ray Ω and an orthogonal coordinate system connected to that ray (see Fig. 2.2). s represents the arclength along the ray Ω from an arbitrary origin, while n represents the distance in the direction perpendicular to the ray. The ray-centered coordinate system is made of $\vec{t}$ tangent to the ray Ω and $\vec{n}$ normal to the ray path at s. The travel time field $\tau(s, n)$ in the vicinity of Ω in this curvilinear coordinate system is given, after Taylor expansion, by the equation (cf. [4]):

$$\tau(s, n) \approx \tau(s, 0) + \frac{1}{2} M(s) n^2 \tag{2.12}$$

where wavefront curvature matrix M(s) is the second derivative of the travel time field in the direction perpendicular to Ω. It is also a solution to the "Dynamic Ray Tracing" equation (cf. [2]):

$$\frac{dM(s)}{ds} + vM^2 + \frac{v_{mn}}{v^2} = 0 \tag{2.13}$$

where v_{mn} is the second derivative of the velocity v with respect to n, in ray-centered coordinates.

This non-linear differential equation can be rewritten using two linear differential equations:

$$\frac{dq}{ds} = vp, \frac{dp}{ds} = -\frac{v_{mn}}{v^2}q \tag{2.14}$$

where p represents the change of the ray's position and direction with the initial conditions, and q represents the change of a paraxial ray's position and direction with the initial conditions (cf. [8]).

Typical output from the ray tracing are traveltime tables for all source, receiver and image point combinations in the inhomogeneous velocity model. These traveltimes then define the weight factor, and phase correction terms in Eqs.(2.9) and (2.10).

2.2 Other tools

2.2.1 The smoothing method

Usually, a Kirchhoff PSDM is performed using the full aperture. This method has an advantage: the high-frequency noise is removed by the summation itself. Indeed, the addition of all the amplitudes, both negative and positive, cancels the sharp variations associated with the incoherent noise and keeps the large amplitudes, that are more likely to be associated with a coherent signal. And the wider is the aperture, the more efficient is this filtering. But the problem is that it also sums the large amplitudes associated with

coherent noise, due to errors made by the ray tracing for example, and many other possible causes to be discussed in the next chapter.

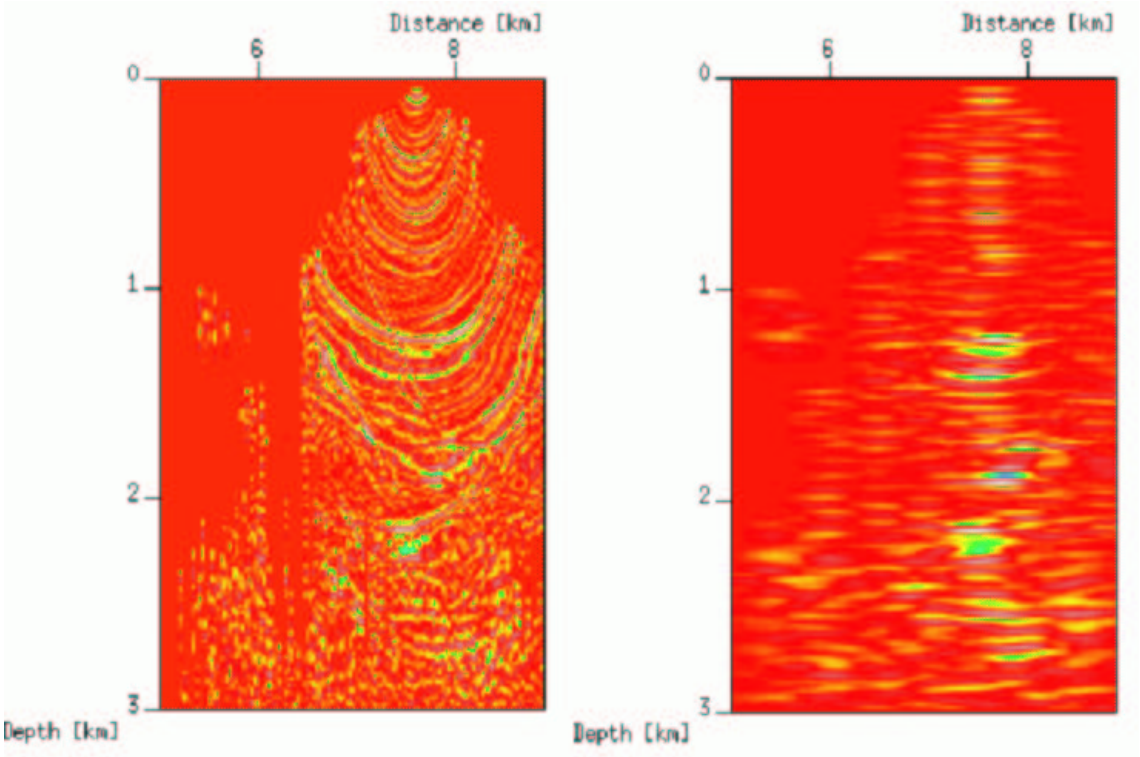

Figure 2.3: Result of the smoothing operation on a Fresnel aperture panel.

Now, in our case, the idea is to limit as much as possible the width of the aperture in order to get rid of this coherent noise. For this reason, we can't use the data without smoothing it first. Indeed, if we add up only a part of a very noisy signal, the result will be very noisy as well. The idea is to introduce a low-frequency filtering of the data which mimics the filtering inherently present in PSDM of full-aperture data.

As an example, consider prestack migration of constant-offset data. To obtain the image along a vertical line through the subsurface, data are summed along time-diffraction curves (cf. section 3.2), corresponding to

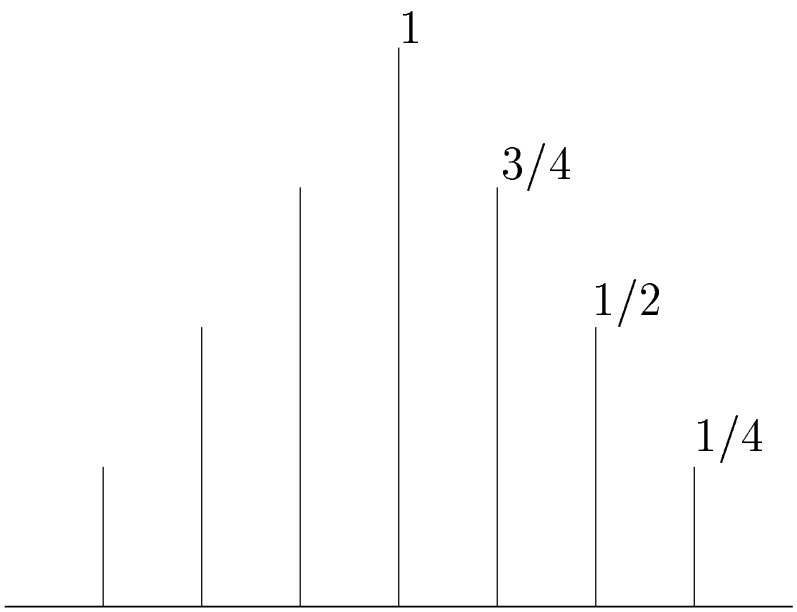

Figure 2.4: The smoothing operator in the case where $k = 3$.

all image depth-points along this line. If we now plot the seismic amplitudes along each diffraction curve, before summation in the horizontal direction, with the vertical axis representing the depth position of each image point, we obtain the panel to the left in Fig. 2.3. This panel is denoted the Fresnel aperture panel, for reasons being more obvious later. Horizontal stacking of this panel gives the image trace along this vertical line. If we low-pass filter the Fresnel aperture panel, we arrive at the result shown to the right in Fig. 2.3. We will later see that this filtered panel plays a vital role in our Fresnel aperture PSDM. Here, we will only state that horizontal stacking of the filtered panel gives virtually the same image trace as for the unfiltered panel. This key observation will be adressed in more details in later paragraphs.

The smoothing method I used is the triangular weighted function. The signal is averaged over a laterally moving interval with a size specified by the user. The size of the operator can be written as $2k + 1$, and the central value has a weight of 1. Then the first neighbouring values have a weight

of $k/(k+1)$, the second adjacent values $(k-1)/(k+1)$, and so on, until the k^{th} adjacent values having a weight of $1/(k+1)$. Then all the weighted amplitudes are summed and the value is put at the $(k+1)^{th}$ sample. Notice that, in order to obtain a signal which is 'true amplitude', we should divide this value by $k+1$. The case of $k=3$ is illustrated in Fig. 2.4.

Chapter 3

The theory

Having introduced the tools needed, I will continue with the theory that lies behind the method of FA-PSDM. I will define some key concepts and present the main feature of the method: the Fresnel aperture selection (cf. [1]). Then, I will explain how it is possible to apply the method in practice.

3.1 Definitions: Specular ray, Fresnel zone and Fresnel aperture

3.1.1 The Fresnel zone and the specular ray

The Fermat's principle states that the correct ray path between two points is the one of least overall travel time. From a mathematical point of view, it can be expressed like this:

$$\tau(s) = \min_{P} \int_{P} s(x) dl^{P} \tag{3.1}$$

where τ is the travel time of the shortest ray path, s the slowness vector (inverse of velocity), P the trial ray path, and dl the unity of distance along ray path.

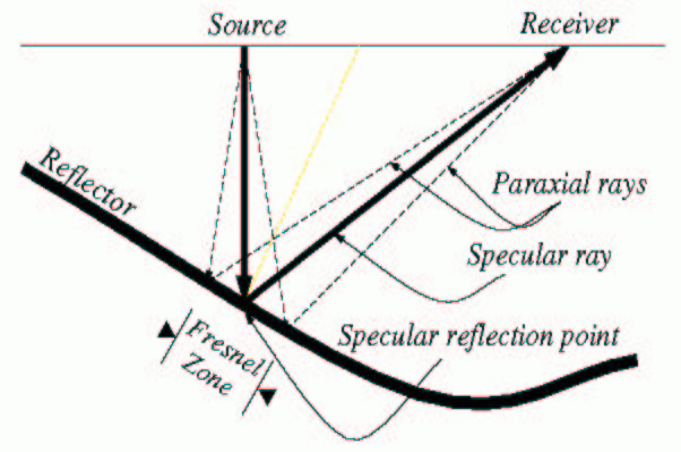

Figure 3.1: Illustration of the specular ray and the Fresnel zone in a single reflection experiment (cf.[3]).

Let us take the simple case of reflection from a single boundary (see Fig. 3.1). What we observe are the specular ray, i.e. the ray that obeys Fermat's principle, and the paraxial rays surrounding it. All these rays form what we call the Fresnel zone.

The Fresnel zone was first proposed in 1818, in order to explain diffraction phenomena using Huygen's principle. The first Fresnel zone is usually defined as the largest reflecting area for which all reflected waves reach the receiver with phase shifts less than π. Indeed, all these rays will constructively interfere. In the case where the source and the receiver are at the same location and the reflector is flat, then the Fresnel zone is a disk with a radius that can be expressed as:

$$r_F = \frac{\lambda}{4}\sqrt{1 + (8z/\lambda)} \approx \sqrt{z\lambda/2} \tag{3.2}$$

where r_F is the radius of the first Fresnel zone, z is the depth of the reflector, and λ the wavelength of the dominant frequency component of the signal.

Hence, when we deal with a band-limited signal, the reflection of the energy not only occurs at the specular reflection point, but involves a whole volume around this point. Indeed, if we consider a signal containing infinite frequencies, then, since there are no paraxial rays in this very case, the Fresnel

zone is reduced to the dimension of a single point: the specular reflection point. Indeed, r_F goes to zero as λ goes to zero in Eq.(3.2).

3.1.2 Kirchhoff summation and the Fresnel aperture

Before we introduce the concept of Fresnel aperture, we give a brief review of the summation principle inherent in Kirchhoff migration.

Consider now the 2-D synthetic data shown in Fig. 3.2. The section represents zero offset traces computed from the velocity model shown in Fig. 3.2-A, using Kirchhoff modeling. In this example, we take one image point, which we denote A (corresponding to the blue spot in Fig. 3.2-A), and we compute its related time-diffraction curve. In practice, this is done using the ray tracing technique to compute travel time tables. The velocity model is the same as the one used to create the synthetic seismic traces. In Fig. 3.2-B, we superimposed this diffraction curve on the seismic section.

Now, the basic principle of the Kirchhoff algorithm is, for each image point of the migrated section, to sum up the corresponding time-domain amplitudes along the time-diffraction curve and put the computed amplitude at the apex of the hyperbola.

Consider an image point located on a reflector (like point A in Fig. 3.2-A), its diffraction curve presents a zone of tangential contact with the zero-offset reflected energy in a region surrounding the point of emergence of the corresponding specular reflection ray at the receiver array. This contact defines the Fresnel aperture (see Fig. 3.3), which is the envelope of the cluster of seismic traces contributing to the image of a common point on the reflector. The term contribute implies that the Fresnel zone of each trace includes the image point considered (cf. [3]). Hence, the Fresnel aperture is the direct time-domain equivalent, at the receiver's surface, of the subsurface Fresnel zone.

So we understand here that only a part of the time-diffraction curve contains the energy scattered by the point of the reflector, while the rest of the diffraction curve only contains energy related to different sorts of noise. This is the concept we introduce in FA-PSDM, where only Fresnel-aperture zones of data contribute.

In the discussion above, we have only considered the zero-offset case, which is the limiting case of constant-offset PSDM. In general, in prestack depth migration, we will consider many offsets, and image each offset separately. If AVO (Amplitude Versus Offset) or AVA (Amplitude Versus Angle) analysis of seismic data are to be carried out, such partial images are important input (eventually resorted into CIP (Common Image Point) gathers). In order to condition the seismic data before such analysis, Fresnel-aperture selection could be used to enhance the signal-to-noise ratio and reduce false events. The potential of the FA-PSDM method will be demonstrated in Chapter 5.

3.2 The Fresnel aperture selection

Consider now more closely the general amplitude variation along a diffraction curve. If we consider a point located on a reflector (see point A in Fig. 3.2), its corresponding amplitude variation along the diffraction curve will include a broad peak, featuring the Fresnel aperture, and some very narrow peaks due to different sorts of noise (see Fig. 3.2-C). While if we consider a point like point B in Fig. 3.4, located somewhere else than on a reflector, we will only observe very narrow peaks (see Fig. 3.4-C). Now we make use of the idea introduced in section 2.2 and low-pass filter these two different signatures employing a smoothing filter (see Fig. 2.4). In the first case (see Fig. 3.2-C), just the broad peak will essentially remain after low-pass filtering, with the narrow peaks being strongly weakened. In the second case (see Fig. 3.4-C), all the peaks will almost disappear and the result is a weak signal. If we now repeat this process for one fixed lateral position along the seismic section and

for each depth sample, we obtain a contour plot like the one shown in Fig. 2.3 to the right. The corresponding unfiltered panel is shown to the left in the same figure and also in Fig. 3.5. Such plots are called Fresnel aperture panels, or migration operator panels. The horizontal stack of a panel gives one image-trace of the depth migrated section (see Fig. 3.5).

One may say that if the signal is modified by the filtering, the resulting migrated image must be different, as far as amplitudes are concerned. Fig. 3.6 shows a prestack depth migrated image (constant-offset of 1500m) of a selected part of the Marmousi model. This model is frequently used to benchmark imaging algorithms and will be discussed in more detail in section 5.1. The image in Fig. 3.6 has been obtained employing the full data aperture and no smoothing of the Fresnel aperture panels. As a comparison, Fig. 3.7 shows the corresponding image obtained when smoothing (i.e. low-pass filtering) of the Fresnel apertures has been applied before stacking to image traces. The differences between the two images are seen to be negligible. The explanation for this phenomenon is that the migration is intrinsically doing the same by summing all the amplitudes one by one, either positive or negative. Another way of illustrating this phenomenum is to run the migration with selected Fresnel apertures without low-pass filtering the data: the result is completely different and very unsatisfactory. The reason is that the migration needs the full aperture in order to achieve the same effect as the 'artificial' low-pass filtering.

Another point to notice is that, for the same depth (i.e. horizontal line in the right part of Fig. 2.3) there sometimes exist several spots that can be interpreted as Fresnel apertures. They are called ghosts and are due to noise, inaccuracies in the velocity field or inaccuracies in the ray tracing. Indeed, if data are contaminated by some low frequency or coherent noise for example, they will appear in the panels. Moreover, velocity uncertainties

will introduce errors in the calculation of travel times and incorrectly move out the amplitudes. It becomes an important issue in the case of a complex model where selecting the correct Fresnel aperture is not necessarily straight forward.

But, on the other hand, these multi-spots can correspond to different true Fresnel apertures in the case of a triplication or multipathing.

In this paper, I have explored the possibility of picking the Fresnel apertures by selecting, as a main criterium, the strongest amplitudes. The underlying assumption is that in most cases, the true coherent energy will be associated with the strongest migration amplitudes, and hence the strongest Fresnel-aperture spots. However, as we will demonstrate in Chapter 5, this pragmatic approach must be used with care. In special, I have investigated if an automatic and interactive process is possible. But, like for the velocity picking process, this needs a certain user interaction.

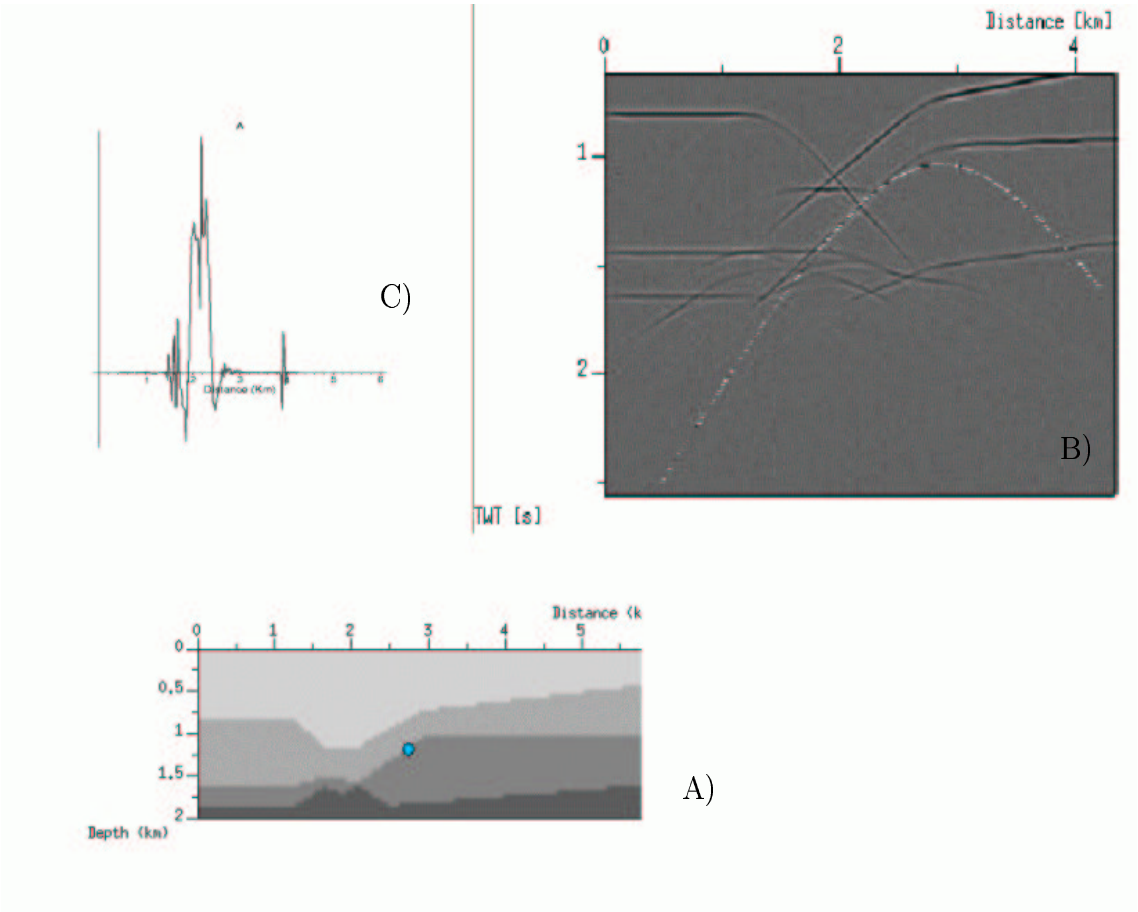

Figure 3.2: A) Velocity model used to compute the synthetic data (note the blue spot representing the point A); B) The time-diffraction curve corresponding to a point located on a reflector superimposed on a zero-offset section; C) Amplitudes along the diffraction curve at point A.

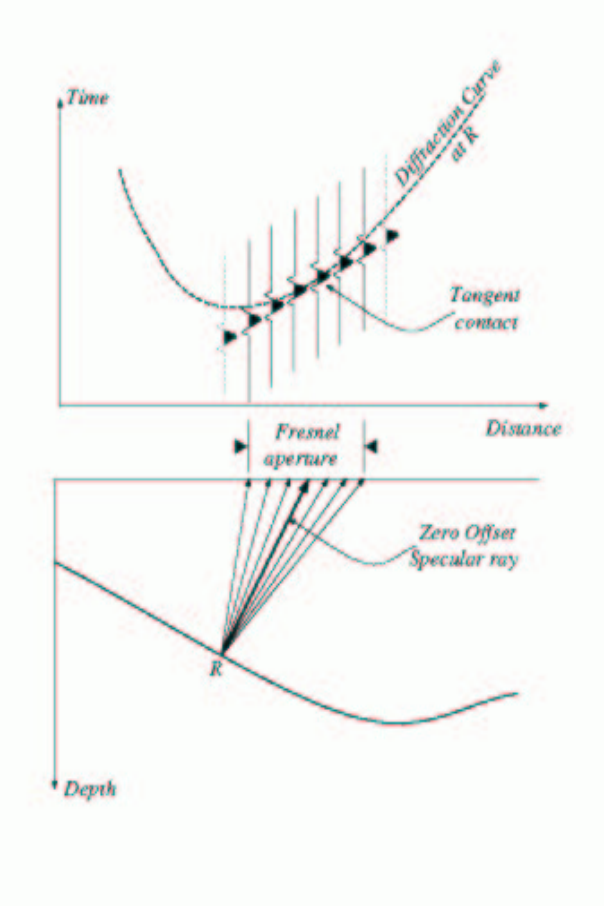

Figure 3.3: Illustration of the link between the tangential contact in the time domain and the Fresnel aperture in the space-domain.

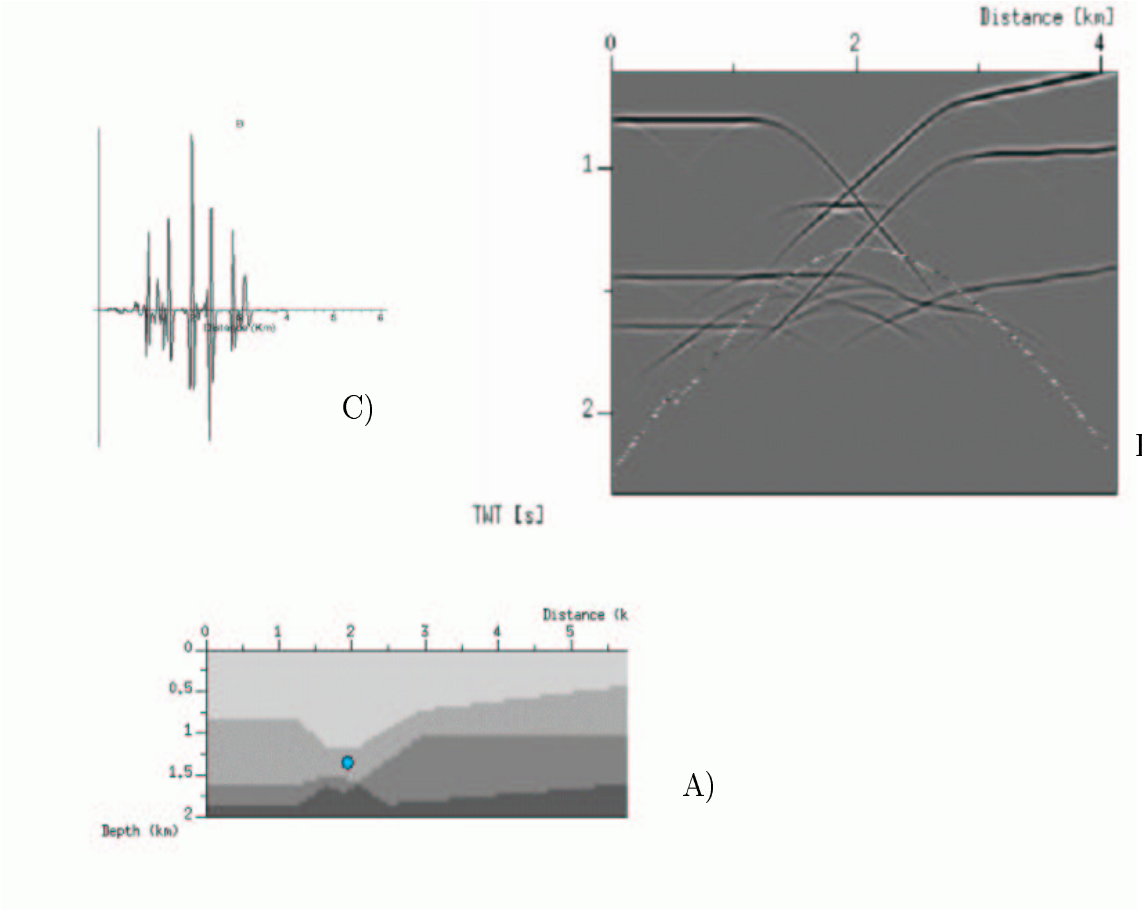

Figure 3.4: A) Velocity model used to compute the synthetic data (note the blue spot representing the point B); B) The time-diffraction curve corresponding to a point not located on a reflector superimposed on a zero-offset section; C) Amplitudes along the diffraction curve at point B.

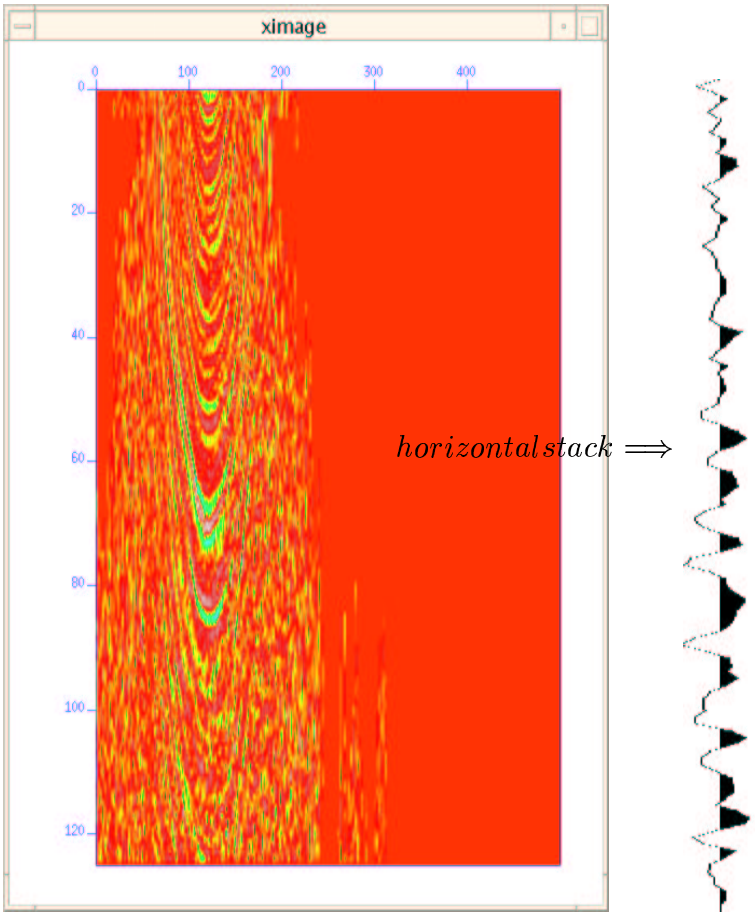

Figure 3.5: Unfiltered Fresnel aperture panel and its resulting image trace.

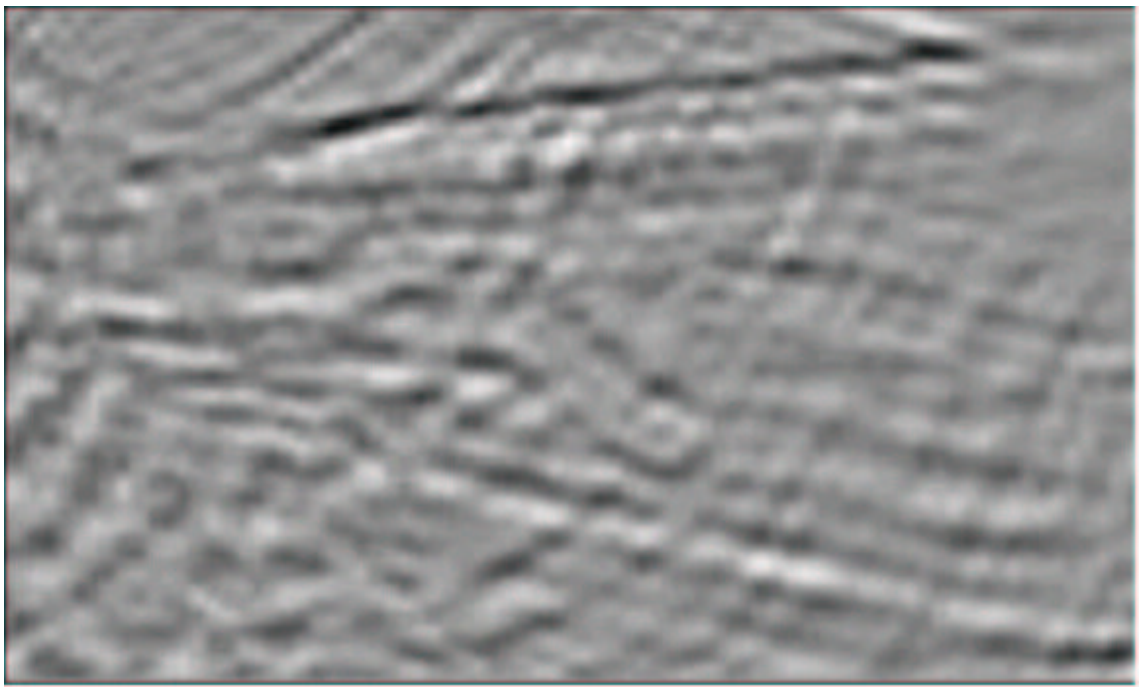

Figure 3.6: Full-aperture PSDM of constant-offset data, from the Marmousi model.

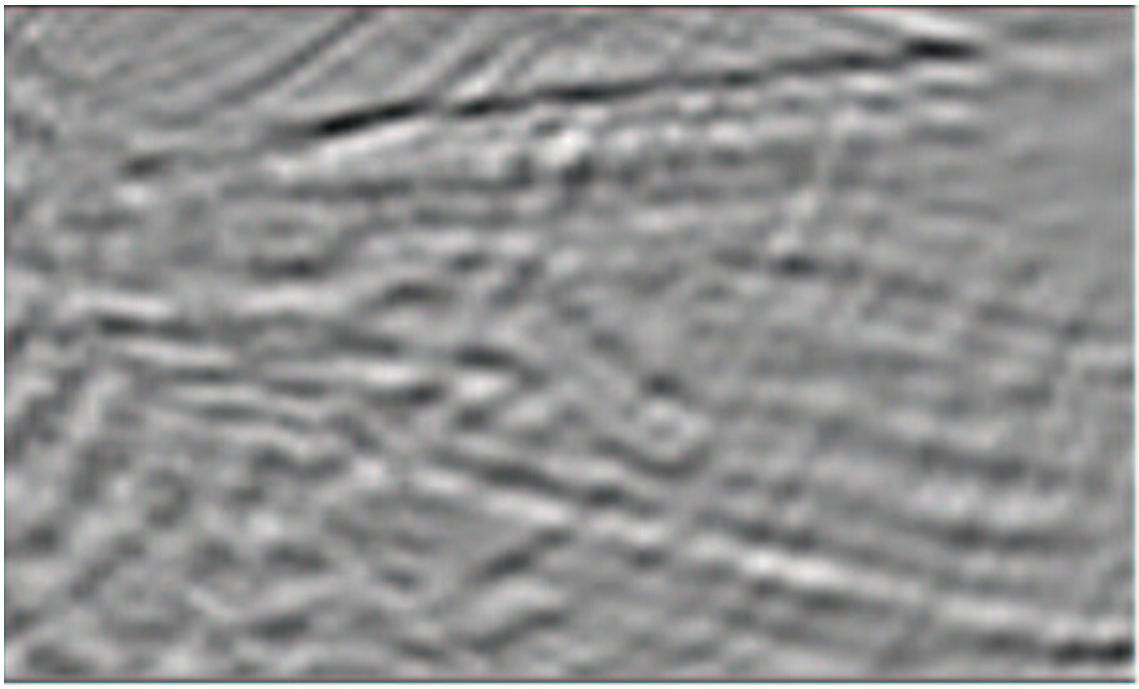

Figure 3.7: Full-aperture PSDM of constant-offset data, from the Marmousi model. The difference with the previous figure is that, this time, a smoothing operator was applied on the Fresnel-aperture panel, prior to the Kirchhoff summation.

Chapter 4

The migration process

In this chapter I present the PSDM process in practice. In the case of Fresnel-aperture PSDM, three tools will be needed: a ray tracing program, a migration program, and a Fresnel-aperture picking program. Both the migration program and the interactive picking software have been developed in this thesis work. But for ray tracing, I used the program *RAYT2D*, which is part of the *SeismicUnix* package (cf. [11]).

4.1 The ray tracing module in SeismicUnix

The ray tracing module from *SeismicUnix*, called *RAYT2D*, calculates travel time tables by 2D paraxial ray tracing. The travel times in shadow zones are compensated by solving the eikonal equation. The input velocity model must be uniformely sampled and smooth in order to avoid the aliasing due to a strong contrast in velocity at the interface between two layers.

As discussed in Chapter 3, a paraxial ray is a ray that is not predicted by the Fermat's principle, but that contributes, by interfering constructively with the specular ray, to the signal recorded at the receiver position. So, the principle of paraxial ray tracing is to compute the travel time of the rays in the neighbourhood of the specular ray by using the Taylor expansion of its travel time. By this mean, the method takes into account the curvature of

the local wavefront, around the central ray (parabolic assumption).

4.2 The migration program

This program, written in FORTRAN90 performs a standard Kirchhoff PSDM using parts of the diffraction curves in the summation process (cf. [1]). It can import the Fresnel aperture picks to migrate the data within narrow apertures, aiming to remove as much noise as possible in order to obtain an optimum image.

4.2.1 Description

The program needs four input files: the seismic data, the interpolated Fresnel aperture picks, the travel time tables, and a parameter file defining the seismic data, the travel time table, and the migration parameters.

It can be used in three different modes:

- computation of the panels used as input to the Fresnel aperture picking software,
- migration of the data employing a full aperture,
- Fresnel-aperture migration.

In the first case, the output is an image file that can be displayed either with the picking software or the *ximage* function of SeismicUnix. As far as the seismic data are concerned, both the SEG-Y format and the SU format can be used as input data formats. The output is written in the same format as the input file.

The program computes constant-offset images. A complete seismic image can be formed by adding these partial images.

4.2.2 The program code

A flow diagram of the program is shown in Fig. 4.1. It consists of three main loops. The first one is indexed on the horizontal samples. Inside this first loop, the second one is indexed on the depth samples. For both of those parameters, their limits are the one of the selected output window. And inside this second loop, the third one is indexed on the seismic traces. This parameter is varying from the very first to the very last trace of the data set.

The outer loop is running over the horizontal positions. For each such position, a depth sample is chosen in the second loop. For each iteration within the inner loop, the program reads the source and receiver positions from the header of the seismic traces (*.dat), then reads the travel time table file (*.ttt) to compute the travel time from the source to the image point and correspondingly for the receiver. Hence, we obtain the total travel time from the source via the image point to the receiver. This value defines the position of the amplitude corresponding to the image point within the trace, and this step corresponds to the depth conversion. The position of the correct amplitude is given by the following relation:

$$\lambda_A = H_r + (k-1)(nt + H_t) + \frac{t_s(k) + t_r(k)}{dt} \tag{4.1}$$

where the position of the sample in the input seismic file is $\lambda_A(x, z)$, the length of the reel header H_r, the length of the trace header H_t, the position of the current trace along the seismic line k, the number of samples per trace nt, the travel time from the source to the image point $t_s(k)$, the travel time from the image point to the the receiver $t_r(k)$, and the sampling interval dt.

Notice that H_r and H_t are fixed values which depend on the format of the input seismic file. The first part of the equation ($\lambda_A = H_r + (k-1)(nt + H_t)$) skips the beginning of the file in order to go to the correct trace, then the remaining term of the equation points at the correct sample within the trace.

This means that, for a given image point with its lateral position and depth, the program has to collect the correct amplitudes composing the diffraction curve by making k vary within the migration aperture accord-

ing to this equation. Notice that $t_s(k)$ and $t_r(k)$ must be updated for each k. Then, the weight factor discussed in Chapter 2 is applied to the sample's amplitude. At the end of the seismic trace loop, the result is the migration operator for a given aperture.

Before the loop over depth samples ends, the migration operator is smoothed using the method previously described, and output to a file. If the type of output chosen was a migration operator panel, also called log-image (*.img), the result is written to a file as it is. In the case of a full aperture, the migration operator is summed and the result written to a file (*.su). If the Fresnel aperture migration is performed, the program reads the pick table file (*.pit) and sums the part of the migration operator centered at the pick location with the aperture specified by the user in the parameter file. After this operation, the loop over the depth samples is completed.

The header of the output migrated trace is updated or the file is closed with a zero in the case of the log-image output (*.img).

Finally, the whole process is repeated for all horizontal positions.

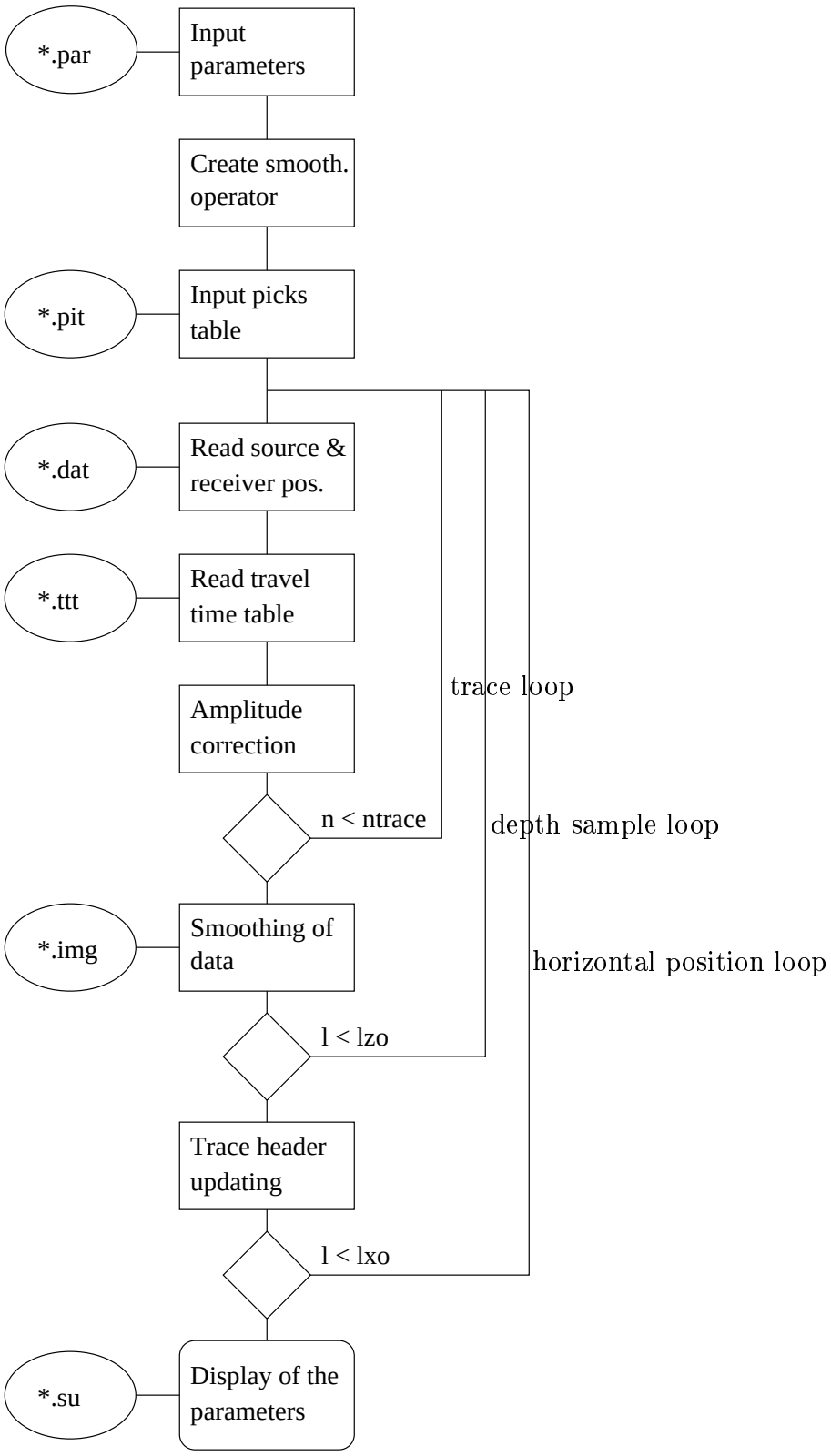

Figure 4.1: Migration program chart.

4.3 The picking software

The picking software was designed using MATLAB. I choosed this option because of the rich choice of built-in functions that are included with the package, especially graphical and interactive ones. The input data are the migration operator panels generated by the migration program (cf. section 3.2). They are uniformly sampled along the seismic line and have been smoothed in order to make the interpretation of the Fresnel apertures easier. The purpose of the interactive picking program is then to select the Fresnel apertures to be used during migration and to interpolate both laterally and in depth the picks so that, to each sample of the seismic section, corresponds a value.

4.3.1 The Matlab built-in functions

First, I will describe the functions from MATLAB that I used to complete this program. The main ones are *imagesc*, *ginput*, and *interp1*.

The function *imagesc* was used in order to display the data stored in a matrix as an image. Each element of this matrix corresponds to a rectangular area in the image. The color of each area is given by the colormap used.

The function *ginput* was used in order to enable the user to select an unlimited number of points from the figure using the computer mouse. It returns the coordinates of the location of the mouse pointer in the same coordinate system as the figure displayed.

The function *interp1* was used in order to interpolate the picks. Indeed, this latter performs a one- dimensional interpolation using polynomial techniques, fitting the supplied data with polynomial functions between the data points and evaluating the appropriate function at the desired interpolation points. There is choice between four different interpolation methods : *nearest neighbour* ,*linear*, *cubic spline*, and *cubic*.

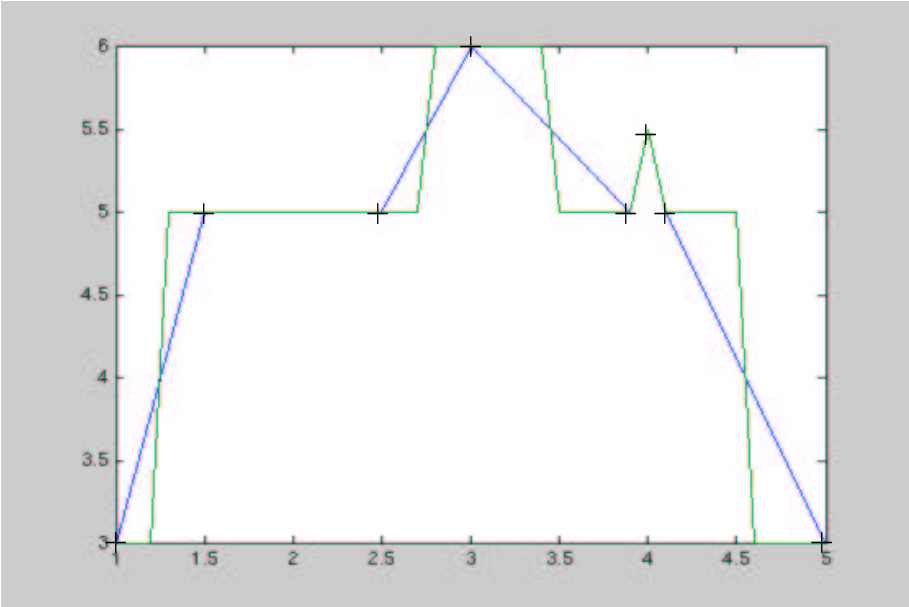

Figure 4.2: Nearest point interpolation (in *green*) compared to the linear interpolation (in *blue*) between eight picked points (+).

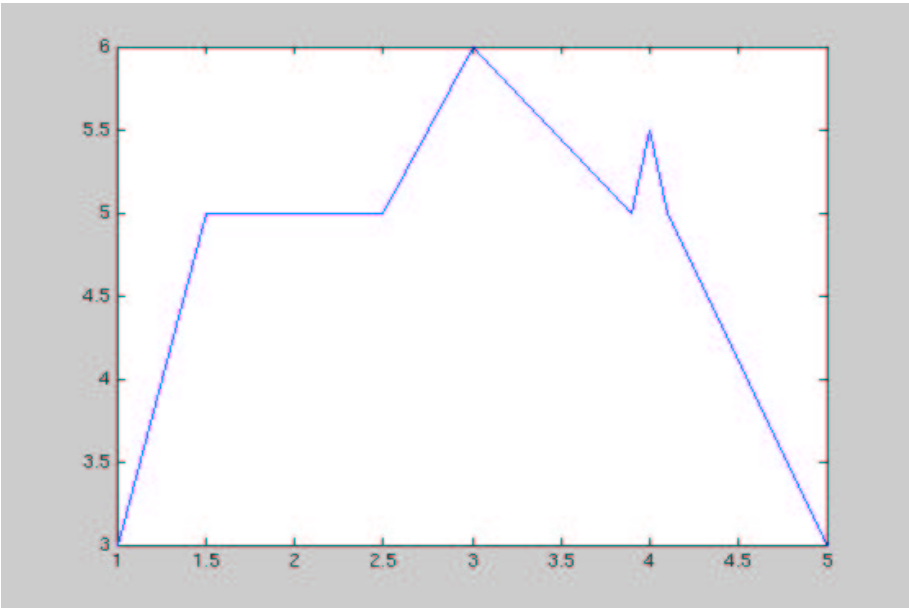

Figure 4.3: Linear interpolation between the same 8 points.

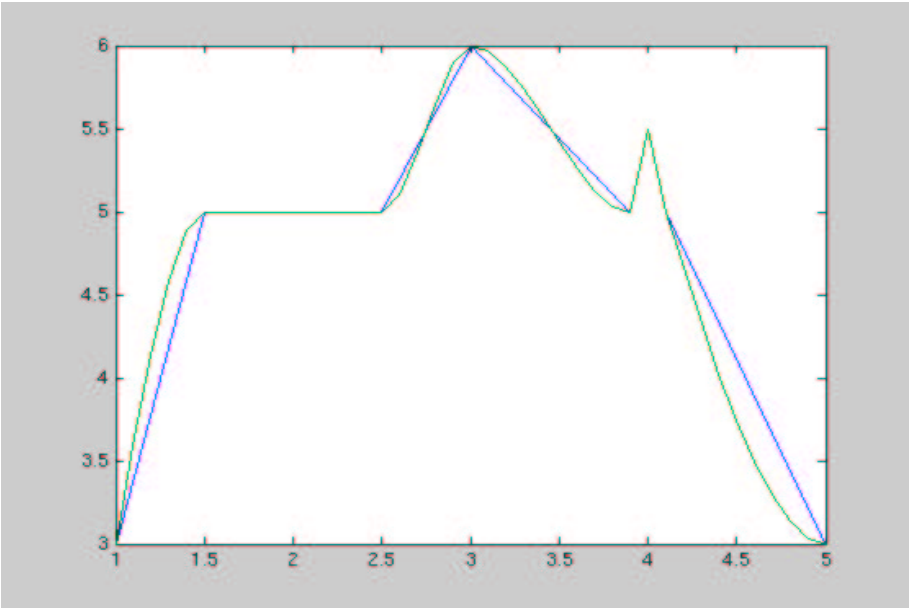

Figure 4.4: Cubic Spline interpolation (in *green*) compared to the linear interpolation (in *blue*).

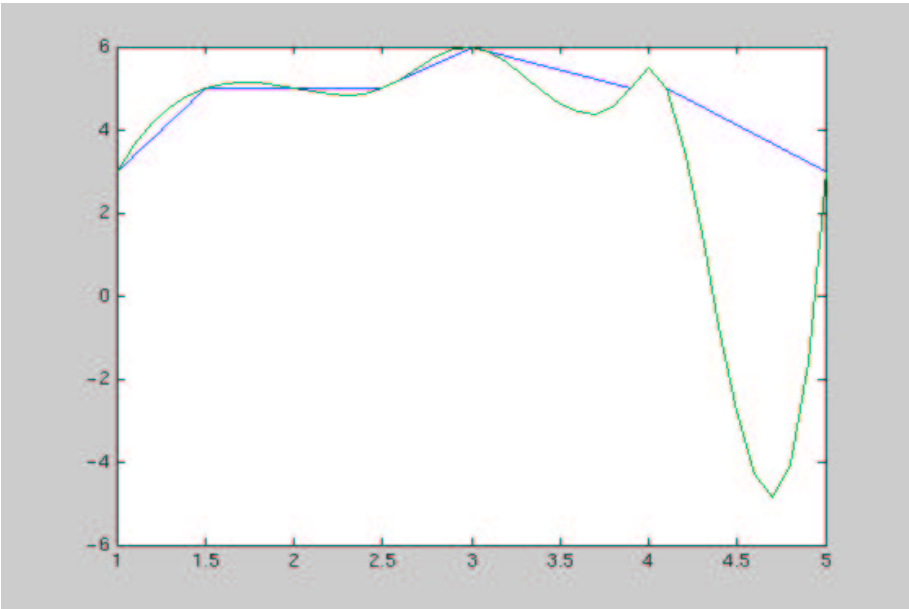

Figure 4.5: 'Piecewise Hermite' interpolation (in *green*) compared to the linear interpolation (in *blue*).

The first method sets the value of the interpolated points to the value of the nearest existing data point (see Fig. 4.2). This is the fastest method, although it provides the worst results in terms of smoothness.

The second method fits a different linear function between each pair of consecutive existing data points (see Fig. 4.3). This technique requires slightly more execution time, but, unlike the nearest neighbour interpolation, it changes in a less abrupt manner. An important feature is that the slope changes at the picked points.

The third method fits a different cubic function between each pair of consecutive existing data points, and uses the spline function to perform cubic spline interpolation at the data points (see Fig. 4.4). This method has the longest execution time, but produces the smoothest results. However, one may obtain unexpected results, if some points of the input data are non-uniformly scattered.

The last method performs a 'piecewise Hermite' interpolation. This method preserves the monotonicity and the shape of the data (see Fig. 4.5), but requires more time than the three first methods. Both the interpolated data and its derivative are continuous. In addition, the points have to be regularly sampled to give a reasonable result. This reason explains the 'overshoot' between the two last points in Fig. 4.5, on the right.

The program uses both the linear interpolation and the cubic spline interpolation: the first one to interpolate the picked points along the depth axis, and the second one to interpolate the points along the horizontal axis. I chose the cubic spline interpolation in the lateral direction because the interval between the points is constant and the changes are more gentle than in the depth direction. Indeed, along the depth direction, sample points are irregular and values can change significantly, so the linear interpolation is more robust. This method is also faster then the cubic interpolation.

4.3.2 The program code

In the actual design of the program, I had to think about the key features this software must have and how to link them together in the program. Then, I had to try to improve the whole code by adding some "user friendly" options.

The first choice was to store the input data in a matrix, instead of reading the values one by one, directly into the file. This has the drawback of requiring more RAM, but simplifies the program and makes the execution quicker.

About the graphical part, one of the main goals was to display both the panel data and the picks from the previous panel superimposed in the same graphical window, so that it would be easier to define a trend along the profile. Moreover, the choice was made to display the values of the input data as their absolute value, so that it would be easier to track the large amplitudes in comparison to the weaker ones, whatever their polarity.

As far as the interpolation is concerned, the data have to be interpolated in depth for each panel, then laterally at the very end of the process. Moreover, I had to decide what kind of interpolation was the best in this case. The linear interpolation was chosen to be performed in depth and the spline method to be performed laterally, like what most of the ray tracing interpretation sofware do to model the horizons.

Furthermore, I introduced an option that enables the user to display all the panels and their picked trends in order to make it easier to follow the global trends along the profile and, eventually, to decide whether it is needed to partly re-pick it. Indeed, it helps to see whether the position of the picks correspond to the direction of the dips expected for each area of the seismic section. But bare in mind that such dip correlation is valid only if the overburden is not too complex.

At the end of the lateral interpolation, all trends are displayed simultaneously as a control of the smoothness of the interpolation performed, and the user can then save the matrix to a file to be used by the migration program.

Finally, I added another option to the program, so that it could edit

the picks stored in a file. Then the user does not need to repick the whole line, in case only a few samples have to be changed and thus, saves a lot of reprocessing time.

4.3.3 The software in practice

In order to illustrate the functionality of the software, a synthetic dataset, known as the Marmousi model (cf. [5]), has been used. This model will be discussed in more details in the next chapter.

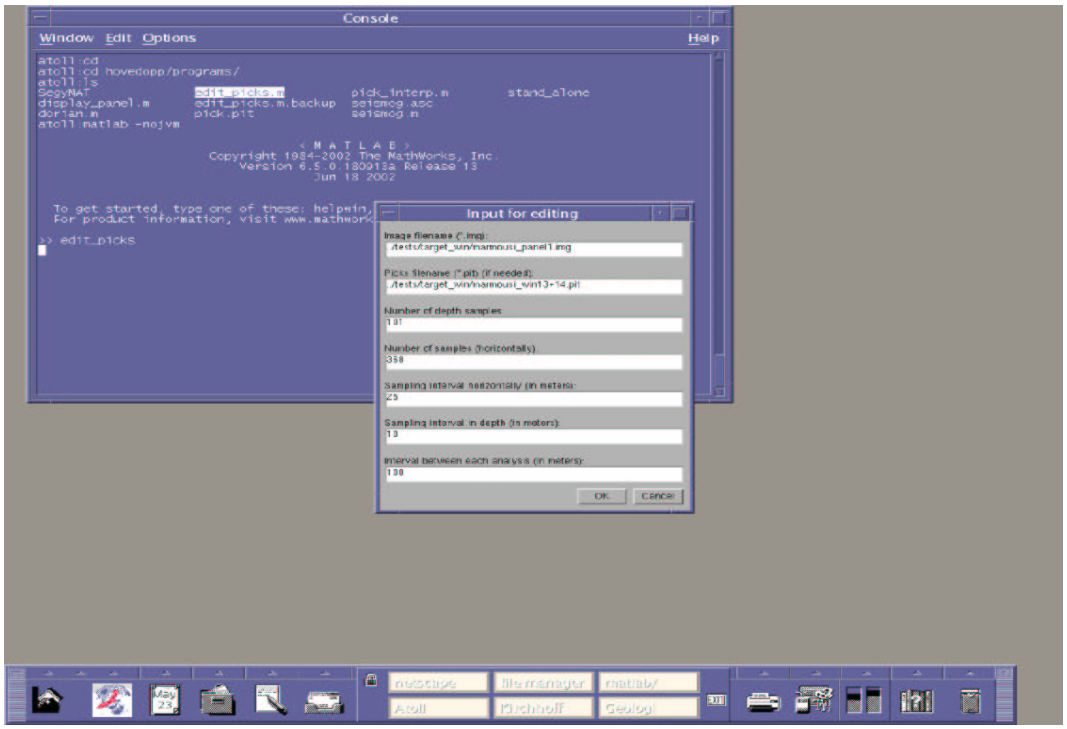

Figure 4.6: Parameters window.

The first step is to open Matlab and run the program script (see Appendix B). A pop up window appears and the user has to fill in the different parameters that the program needs in order to read correctly the input file

and perform the interpolation according to the parameters of the dataset (see Fig. 4.6).

Then, the first panel is displayed, with a small window superimposed indicating some informations (see Fig. 4.7). This window will be opened automatically every time a new panel is being displayed. This is due to a feature of *ginput* that causes that the first pick is not always recorded. So the user has to click OK in order to continue the picking.

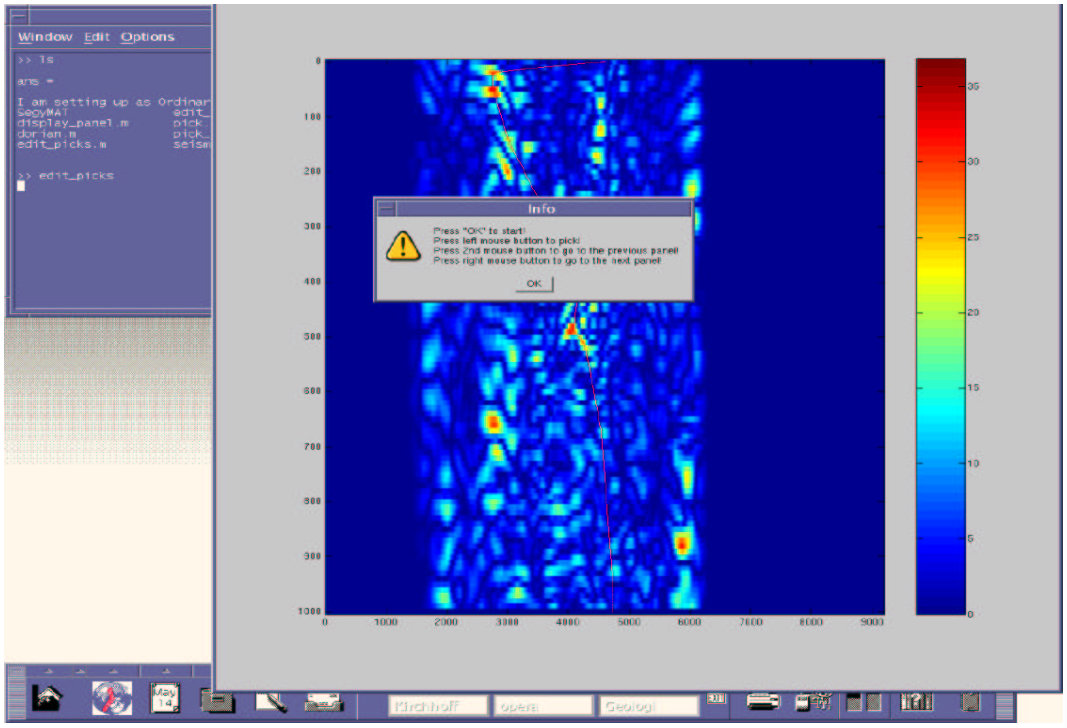

Figure 4.7: Start picking

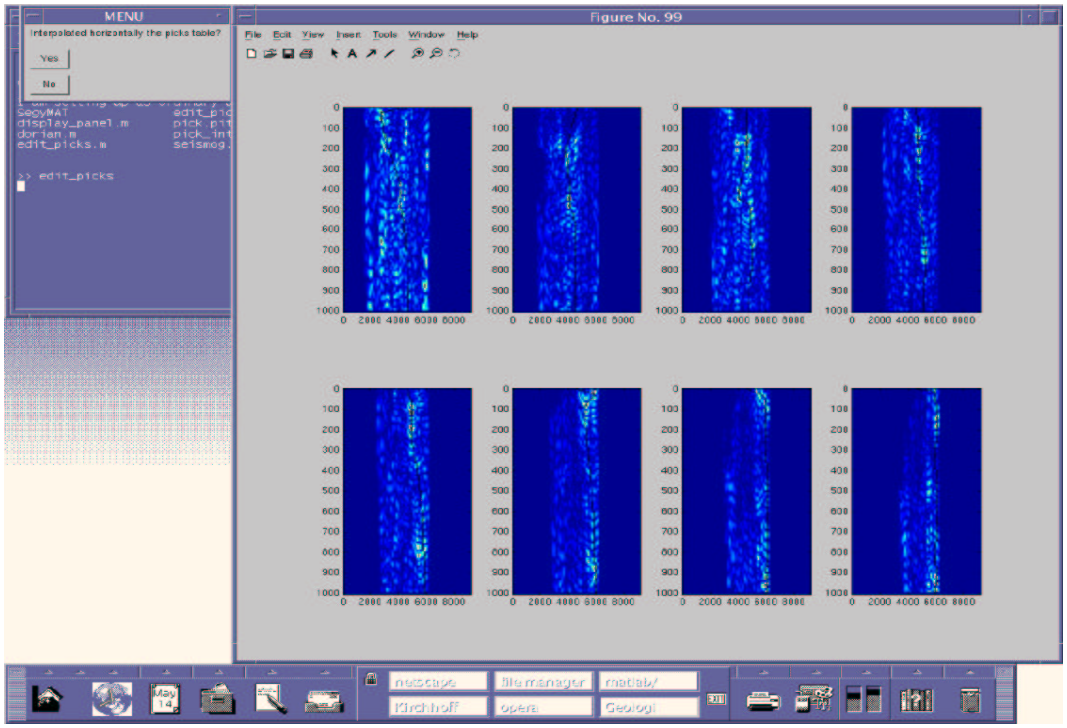

Figure 4.8: Panels display.

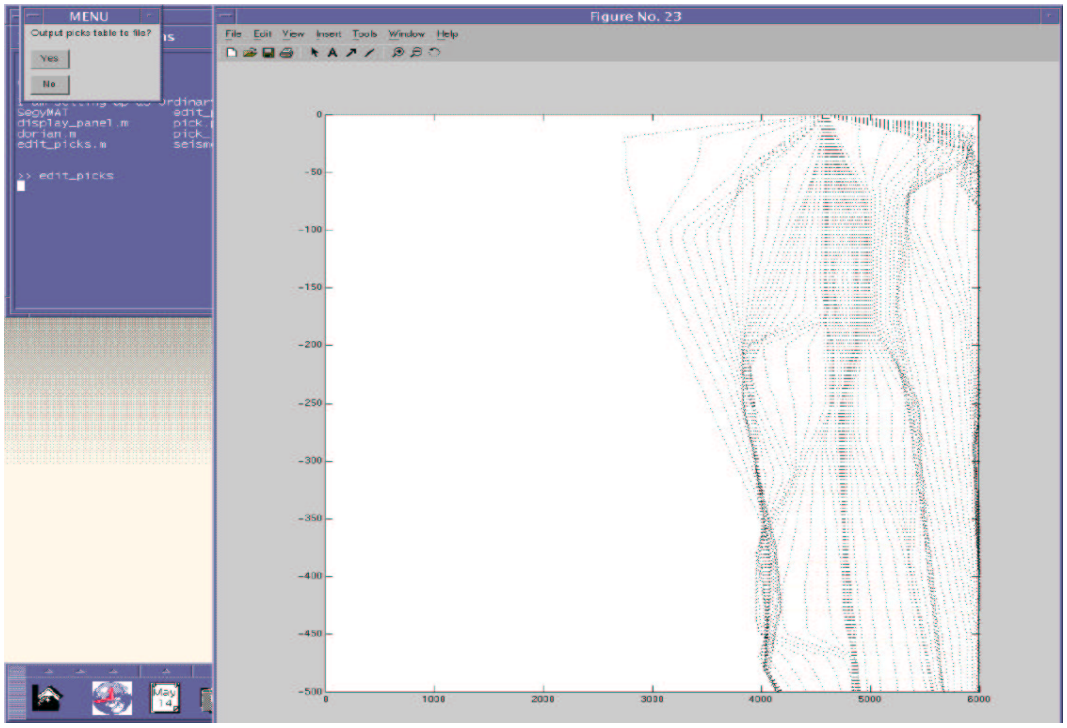

Figure 4.9: Interpolation result display

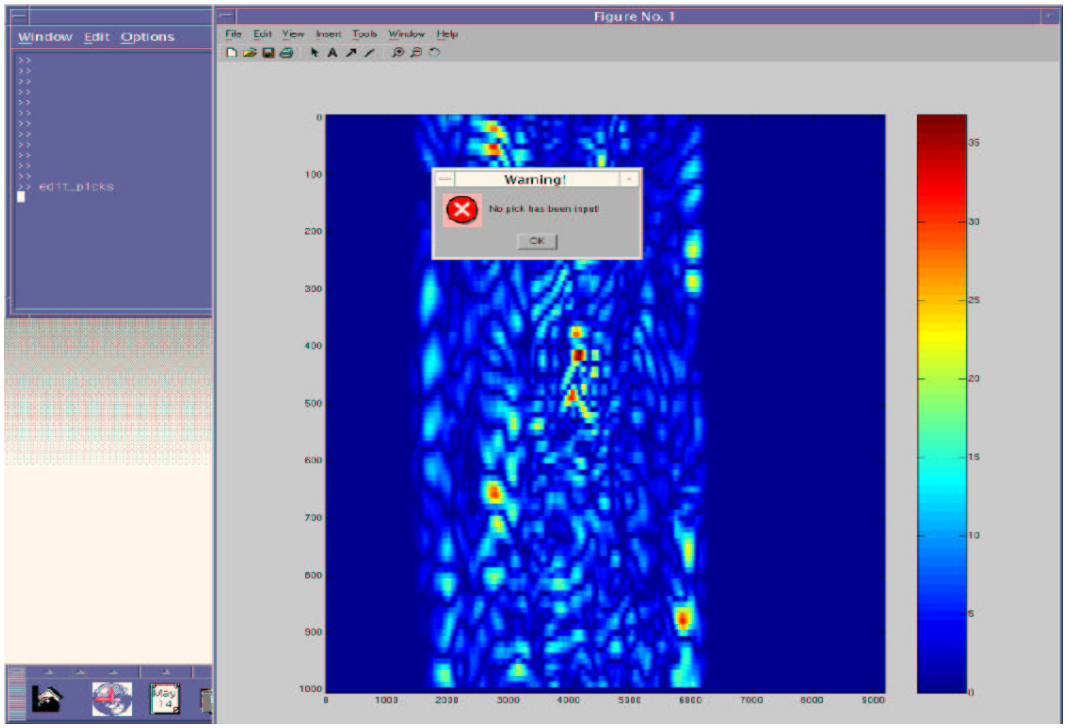

Figure 4.10: Error message.

In the case if no pick at all has been recorded for a panel (see Fig. 4.10), it is not possible to return to a previous panel. The mentioned feature prevents any mistakes in case, for a given reason, *ginput* did not work as expected. However, the warning window disappears after a few seconds and the user should not click on it, since the point would be recorded by *ginput*!

When all the panels have been picked, the program gives the opportunity to display all the panels and their picks in the same window (see Fig. 4.8). This option provides the user with an overview of the trends he followed along the seismic line.

Then, the user has the choice between stopping the process if he wants to change the trend and re-pick, or start the lateral interpolation of the picks, i.e. between all the panels being picked. This step is the most time consuming, and depends on the record length and the length of the line. At completion, the result is displayed in a new window where all the trends are superimposed (see Fig. 4.9).

Finally, after having checked that the interpolation is properly done, the user can save the result as an *ascii* file which can be used as input to the migration program. This file can easily be checked or manually edited employing a simple text editor.

The interactive program described in this section has now all the options required to efficiently pick the Fresnel apertures and thus, actually looks pretty much like a velocity picking software. It has enough features to perform the picking on a large dataset without having any serious problem or giving rise to prohibitive large computing times.

Chapter 5

The application

In this Chapter, the actual performance of the FA-PSDM method is being demonstrated. I used two datasets: one is the complex synthetic dataset known as the Marmousi model created by the IFP which is often used as benchmark for testing of imaging methods. The second dataset has been kindly granted by CGG Norge and is a 2D-line from an area in the North Sea featuring a salt dome.

5.1 The Marmousi model

This is a famous data set often used to benchmark processing algorithms in seismic because of its complexity. Indeed, it contains many reflectors, steep dips and strong velocity gradients, both vertically and laterally.

5.1.1 Presentation

Originally, it was designed by the Institut Francais du Pétrole in 1988 and led to a workshop organized at the EAGE meeting in 1990 (cf. [5]). The overall goal was to compare the results obtained by the different participants, who were given the dataset as a blind test. The Marmousi model was inspired by a real data set from the North Quenguela Trough in the Cuanza Basin in Angola, and is featured by two geological phases.

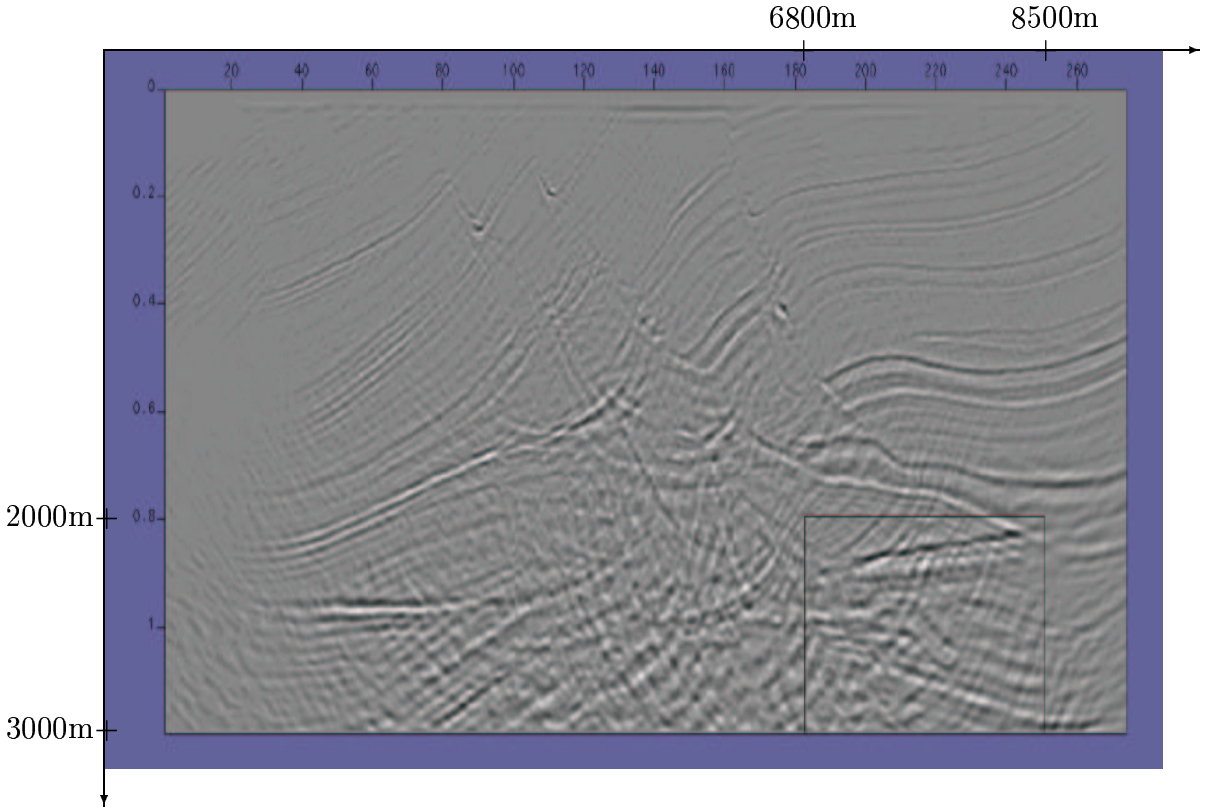

Figure 5.1: The marmousi synthetic data-set.

First, the continuous sedimentation of marls and carbonates (see Fig. 5.1). These sediments were then slightly folded and eroded. The second is made of saliferous evaporites overlayed by a clayey-marly series. Then a thick deposit of shaly-sandy detrital sediments whose facies thickness was connected to continuous lateral creep of the salt due to the overburden pressure. This latter phenomenum caused the uneven lateral repartition of the salt and the appearance of slanting growth faults which were active during all this second phase.

The part of the model I selected in this thesis is located between 2000m and 3000m in depth. This part of the model is challenging since the complexity of the overburden makes it difficult to obtain an accurate image employing

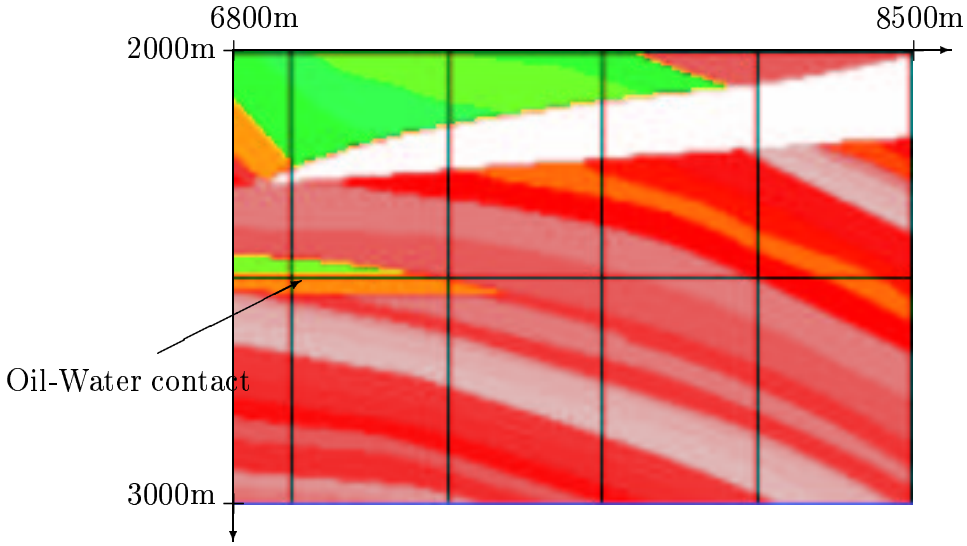

Figure 5.2: Velocity model in the area of interest.

a conventional PSDM algorithm, especially when considering constant-offset images. The most interesting zone is located between 6800m and 8500m, laterally. It includes toplapping and downlapping events, strong velocity contrasts, and the target zone representing an oil-water contact.

5.1.2 The full aperture migration

Inspection of the velocity model (see Fig. 5.2) shows that the most complex part of the zone of interest are on the left side. Due to the complexity of the overburden, we expect the ray tracing to do errors in its approximation of the travel times. In addition, we employ a smoothed version of the true velocity field as a background model. We therefore expect the full-aperture migration to experience difficulties.

By looking at the full aperture PSDM (see Fig. 5.5) for the offset of 1500m, one can easily notice the image being corrupted by noise. Indeed, in the upper part of the image, the strong events dipping towards the left are not real. This left-dipping noise can be seen in all parts of the image, giving an overall distored reconstruction of the zone of interest.

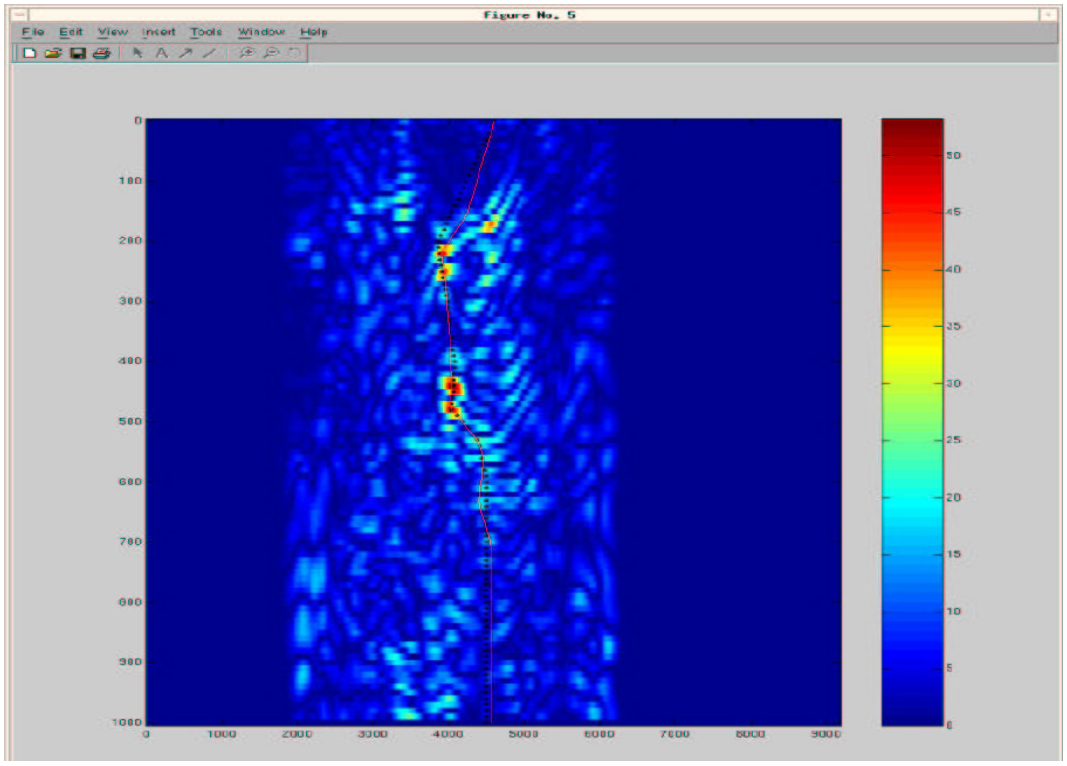

Figure 5.3: picks panel.

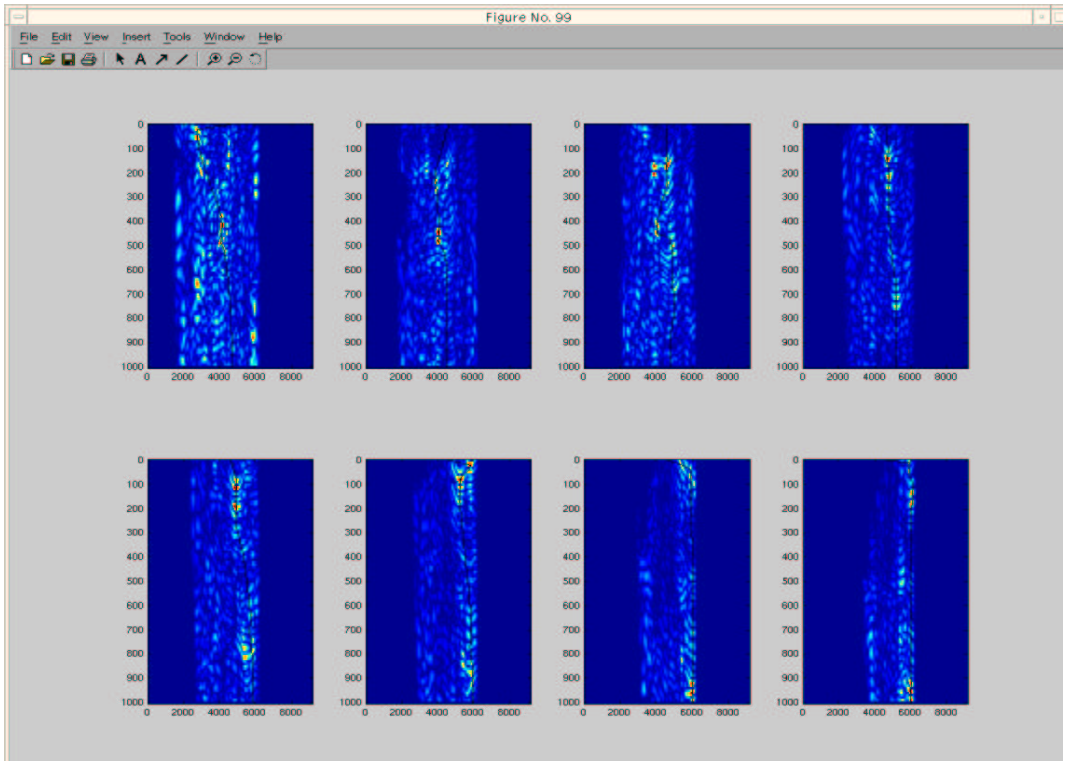

Figure 5.4: Picked trend along the window.

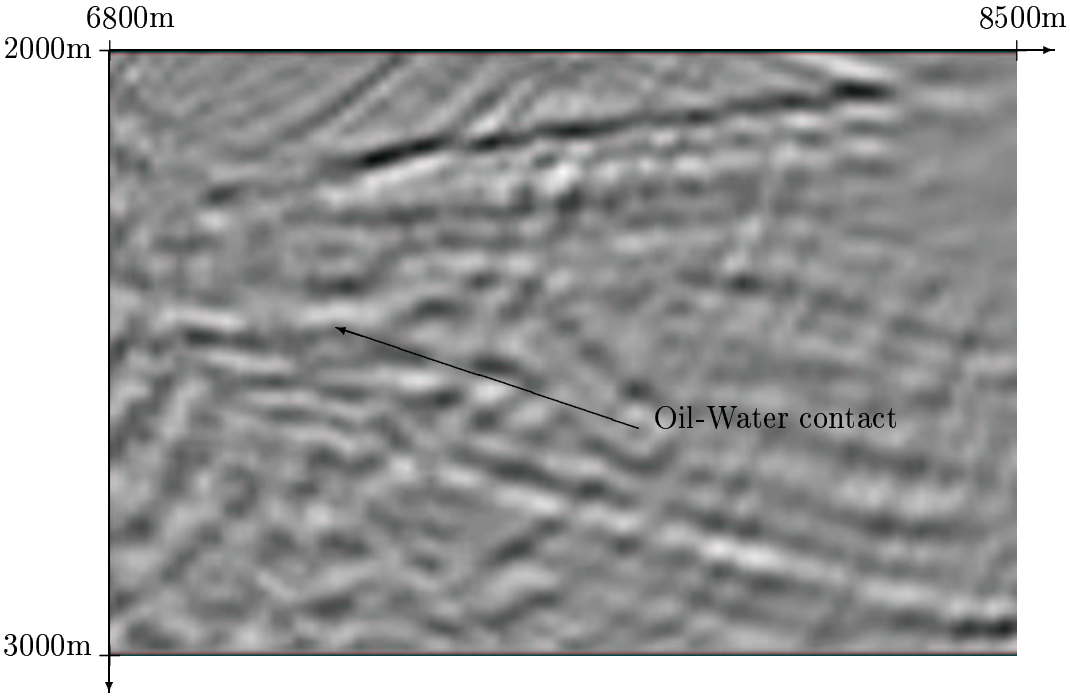

Figure 5.5: Full aperture migration result (compare with Fig. 5.5).

Furthermore, the oil-water contact is rather blurred and difficult to interpret.

In the bottom left corner, the image is dominated by low frequency noise that prevents any interpretation of this area by hiding the actual dipping horizons beneath the oil-water contact.

5.1.3 The Fresnel aperture migration

The overall goal of the FA-PSDM is to remove false coherent events present in the full-aperture migrated image, caused by errors in the velocity model, imperfections in ray tracing and other noise sources. Fig. 5.3 shows the example of one Fresnel aperture panel for this data set, with superimposed picks (representing the centers of the Fresnel apertures). Correspondingly, Fig. 5.4 shows the picked trend along the image aperture. Based on this analysis, the improved image was obtained in Fig. 5.6. Indeed, all the

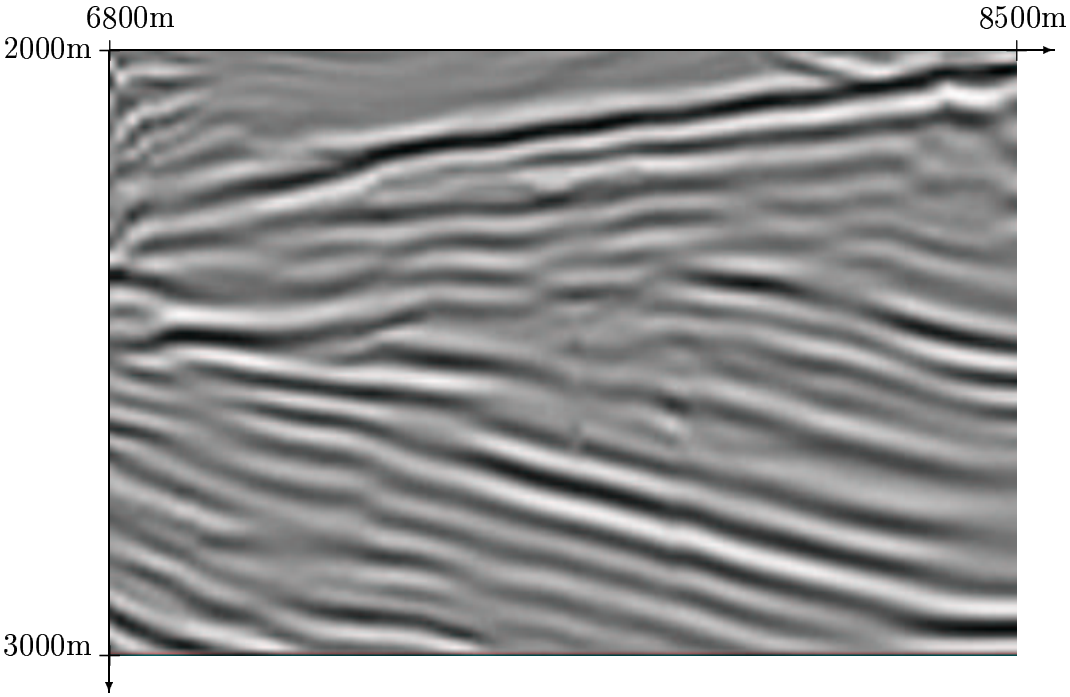

Figure 5.6: Fresnel aperture migration. Note the water-oil contact that is clearly visible.

false left-dipping events have been removed from the migrated image, and most of the random noise as well (compare with Fig. 5.5).

The extension of the flat-spot is now easier to interpret and it is even possible to see the top-lapping horizons.

All the low frequenciy noise has been removed in the bottom left corner, and the dipping events beneath the target zone are now visible.

Note that the effect of the FA-PSDM in this data example is partly similar to a dip-filter. However, the unwanted noise is removed in a physical consistent manner, and unlike the effect of a FK-filter, the data are not smeared. The application of a FK-filter to the image shown in Fig. 5.5 gives a much poorer result than Fig. 5.6, as shown in [3].

5.1.4 Discussion

This example of FA-PSDM illustrates one of the main features and advantages of this method: it removes non-physical coherent noise, including dip-

filtering. The difference between the conventional PSDM and the FA-PSDM is quite striking. But it is important to notice that this feature can be a pitfall too. Indeed, if one choose to pick only on the maximum amplitudes in the panels, there is a problem in cases where the noise is stronger than the real events. This can be seen in the top left corner where the left-dipping noise turns out to be stronger than the true right-dipping horizons and only the noise remains on the FA-PSDM migrated image.

5.2 Field data

This data set was granted by CGG Norge and is located somewhere in the North Sea featuring a salt dome truncated by more or less horizontal layers (see Fig. 5.7).

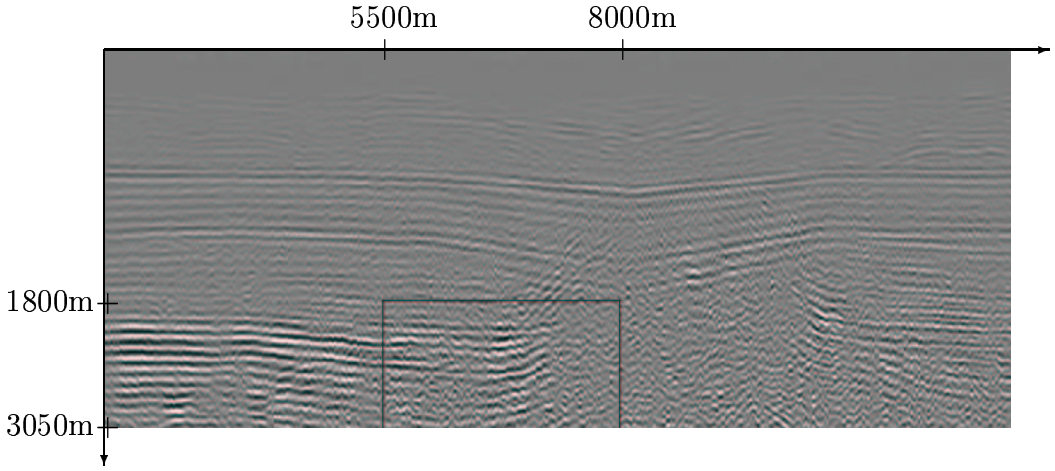

Figure 5.7: Salt dome data-set

The part of the data set used in this thesis is located between 1800m and 3050m of depth and between 5500m and 8000m along the profile. I chose this area in order to test the possibility of improving the accuracy of the migrated image along the flanks of the salt dome. Indeed, it is very difficult to image the termination of the layers, because of the strong diffraction noise caused by the roof of the dome and the strong contrast in velocity. One can

notice that the data are contaminated by some low frequency noise and some dipping diffraction noise.

5.2.1 The aperture zone picking

On the left side of the zone of interest, all layers are almost horizontal. Hence, all the Fresnel apertures appear to fall along a vertical line right beneath its image location (see Fig. 5.8). The difficulty here is the low-frequency noise appearing close to the salt dome, and the left-dipping diffraction noise produced by the roof of the salt dome. These two different kind of noise have stronger amplitudes than the signal itself. In this case, if the maximum amplitude criterium is being used to pick the Fresnel apertures, the final result will amplify the noise and the primary signals will be removed if not included in the aperture. That is why the picking has to take into account the dips. This is possible here since the layers in the overburden are more or less horizontal.

5.2.2 The full aperture migration

In the computations we considered a constant-offset of 1533m (the actual offset range being between 108m and 3083m) When we used the full aperture migration on this data set (see Fig. 5.9), we encountered two major problems that reduced the resolution of the image: the low-frequency noise visible in the upper-right corner of the reconstruction and the diffraction noise caused by the salt dome and its strong contrasts in impedance. Indeed, both phenomena mask the termination of the reflectors at the flanks of the salt dome. This is a crucial point when carrying out the interpretation. In addition, the image is corrupted by the same type of 'cutting-through' noise as observed in Fig. 5.5.

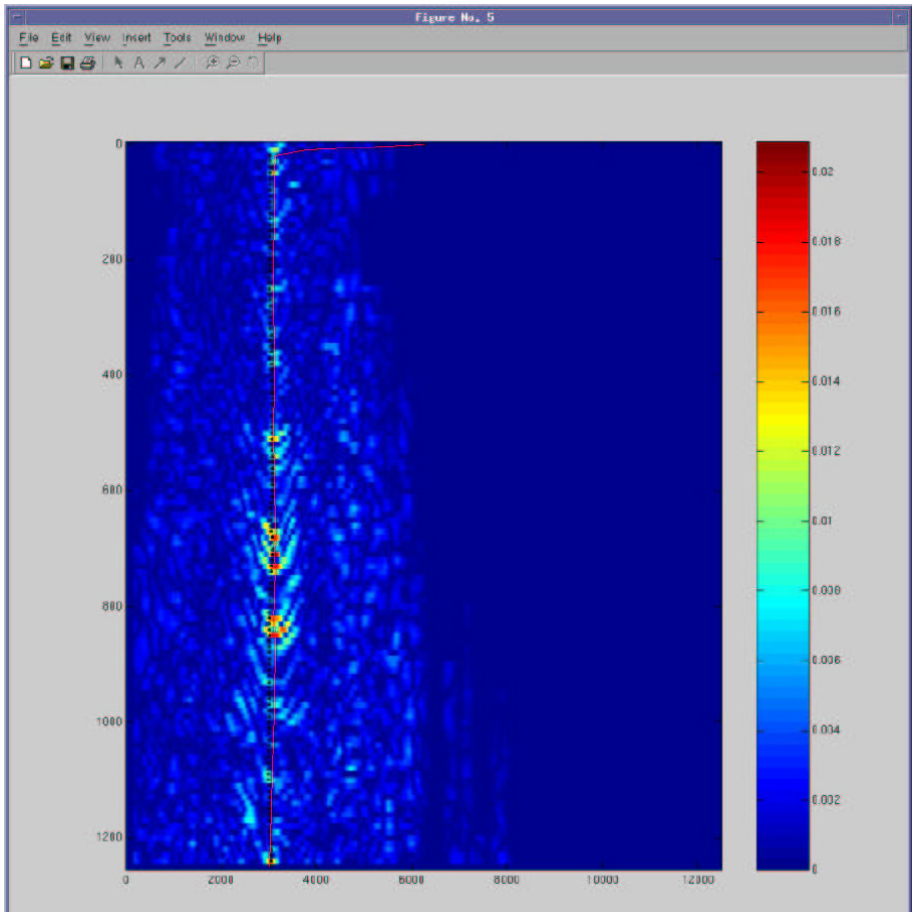

Figure 5.8: Fresnel aperture panel with the picked trend superimposed.

5.2.3 The Fresnel aperture migration

The first image (see Fig. 5.10), is based on picking the maximum amplitudes. We can notice that the two issues discussed above have not been fully corrected for due to the narrow aperture used: the noise, close to the flank of the salt, is still too strong and was enhanced relatively to the real events in the migration. In this case, the only solution is to correct the picks manually. But note that the overall image resolution has improved considerably, removing the 'cutting-through' noise.

Replacing the maximum-amplitude criterion with a user interaction gives the improved result shown in Fig. 5.11. It is now possible to track the

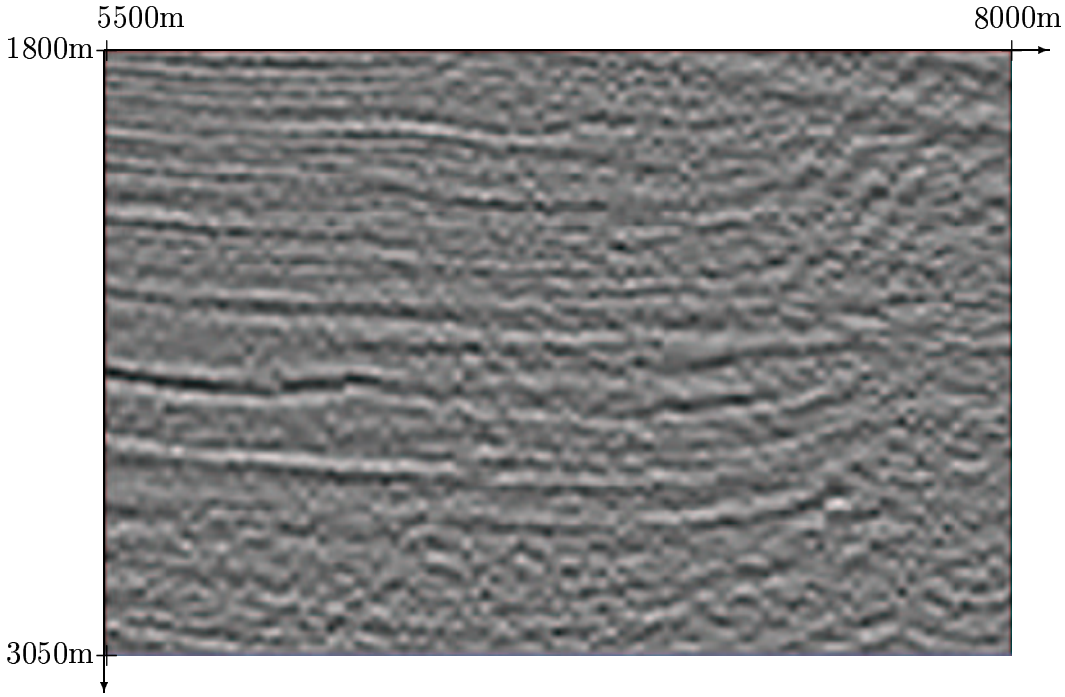

Figure 5.9: Full aperture migration.

termination of the horizons and greatly improving the interpretations. The reason for this improvement is that the diffraction noise has a steep dip compared to the true reflectors which are almost horizontal. Hence, this fact can be used as a guidance when repicking the Fresnel apertures.

5.2.4 Discussion

Both the synthetic data set and the field data set contain features which produce poor results while using the full aperture Kirchhoff migration. For the Marmousi data set, it is due to a complex model giving rise to uncertainties in velocity and ray tracing. In the case of the salt dome, real noise like diffractions coming from the roof of the salt dome mask the real reflection events. In addition, the same 'cutting-through' noise is observed as for the Marmousi case.

This data example demonstrates several advantages of the Fresnel-aperture selection method: it can remove the 'cutting-through' noise caused by imperfections in the velocity model and ray tracing as well as multipathing (here, only constant-offset data are considered, which are more sensitive), but it

can also act as a dip filter. Indeed, as explained before, depending on the dip of the event, it will appear on one side or the other of the apex of the diffraction curve, along which the amplitudes are summed. In other words, if, at a given depth, two amplitude anomalies can be spotted on the Fresnel aperture panel and that the summation aperture is narrow enough to mute out one of them, only the event connected to this dip will be visible on the migrated image. Especially in this last example, we have seen the efficiency of this characteristic.

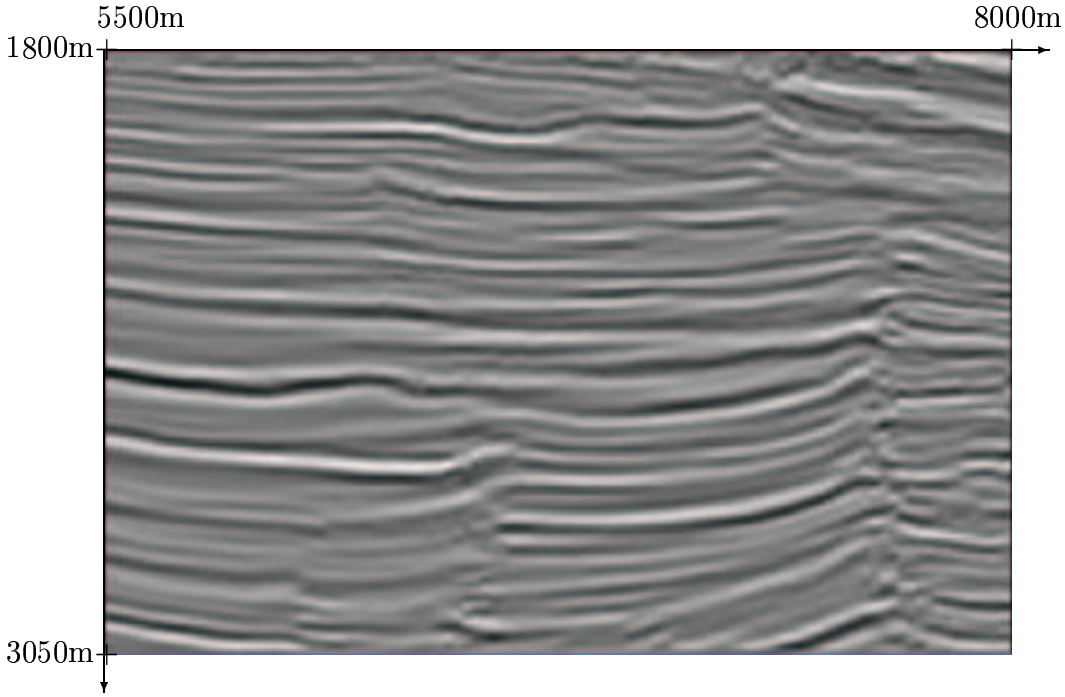

Figure 5.10: Fresnel aperture migration with maximum amplitude as selection criterium.

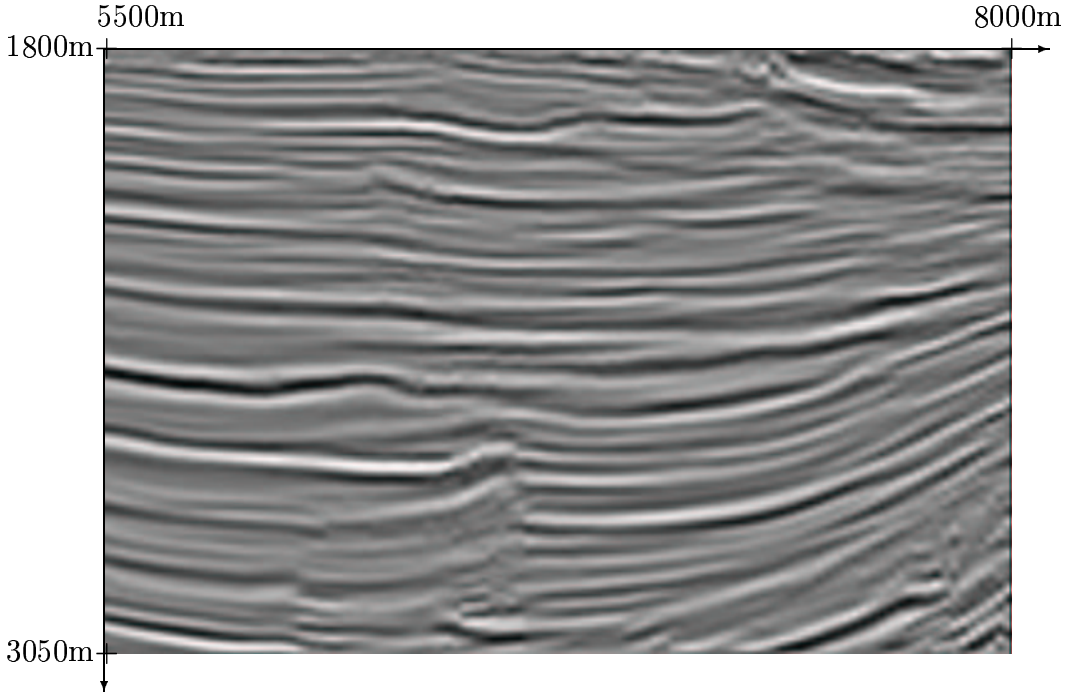

Figure 5.11: Fresnel aperture migration with selection corrected by the user.

Chapter 6

Conclusion

The basic principle of the FA-PSDM method is the fact that only a part of the diffraction curve really contains usefull information about the subsurface. The combination of a simple smoothing of the seismic data, and the concept of Fresnel apertures can give a significant improvement of the S/N ratio in the final image. The FA-PSDM has two key features:

- dip filtering,
- removal of the 'cutting-through' noise caused by imperfections in the velocity model, ray tracing (Green's function computations), multi-pathing, multiples, etc., especially in cases involving a complex overburden.

When we talk about seismic processing in practice, the turnaround of a process has also to be taken into account. Here, we run the PSDM twice; the first time to output the log-image used to pick the Fresnel apertures, the second run to compute the FA-PSDM. The only difference between the two computations, is that during the second run, one inputs the Fresnel aperture picks and performs the horizontal stack of the traces at the end (see 2.1). Then, there is the picking process, which has its analogy in velocity picking. The time needed to pick a complete dataset depends on:

- how coarse is the grid of the locations to pick,

- the quality of the data: clean data and an accurate travel time estimation through ray tracing will reduce the time needed to find the correct trend and discriminate the noise from the real geological events,

- the complexity of the geology in the area.

One parameter should be tested in more detail: the smoothing, or degree of low-pass filtering, of the seismic data before migration. Indeed, too little smoothing can yield a noisy image, while too much smoothing will give an image that will seem smeared. But again (cf. section 2.3), this process is essential to compensate the lack of window data because of the narrow aperture. Without it, the image would look sharper, but contaminated by some random noise. The narrower the aperture is, the smoother the seismic data should be, and the link between these two has still to be investigated further in order to treat this kind of noise.

An automatic implementation of the interactive picking has not been tested here, for example based on some useful criteria like maximum-amplitude and proper geological constraints. It would be of interest to evaluate the possibilities to speed up the process by using such an approach. But, like for the velocity picking, the human intervention will be difficult to eliminate, so a certain user interaction is needed.

To consider the industrial use of the FA-PSDM, the comparison with modules used by the seismic data processing companies in connection with Kirchhoff PSDM should also be done. For instance, the *Compagnie Générale de Géophysique* has implemented a dip model input to its Kirchhoff PSDM module. With this option, the input dip model is assumed, so that the spectral content of the dip events is better preserved and imaged by the algorithm (cf. [9]). It would be interesting to compare the FA-PSDM with this method in terms of quality of imaging as well as in terms of turnaround.

Bibliography

[1] H. Tabti and L.-J. Gelius:*Fresnel-Aperture PSDM*, EAGE 64^{th} Conference and Exhibition, Expanded Abstract, 2002

[2] J. Pulliam and R. Snieder: *Ray perturbation theory,dynamic ray tracing and the determination of Fresnel Zones*, Geophysical Journal International 135;2, p.463-469, 1998

[3] H. Tabti,L.-J. Gelius and T. Hellmann: *Fresnel-Aperture Prestack Depth Migration*, First Break 22, p.39-46, march 2004

[4] B. Beydoun and T.-H. Keho: *The paraxial ray method*, Geophysics 52;12, p.1639-1653, 1987

[5] R. Versteeg: *The Marmousi experience: Velocity model determination on a synthetic complex data*, The Leading Edge, p.927-933, September 1994

[6] M.-F. Sullivan and J.-K. Cohen: *Pre-stack Kirchhoff inversion of common offset data*, Geophysics 52;6, p.745-754, 1987

[7] J.-A. Dellinger,S.-H. Gray,G.-E. Murphy and J.-T. Etgen: *Efficient 2.5-D true amplitude migration*, Geophysics 65;3, p.943-950, 2000

[8] V. Čeverný: *Ray tracing in a vicinity of a central ray*, SEP Reports 28, Stanford University, 1981

[9] A. Pica:CGG,1996

[10] N. Bleistein: *On the imaging of reflectors in the Earth*, Geophysics 52, p.931-942, 1987

[11] Center for Wave Phenomena: *The SeismicUnix homepage*, http://www.cwp.mines.edu/cwpcodes/, version 3.4, 2003

Appendix A

Migration program

```
PROGRAM tomdsm

!**********************************************************************
! Program for Kirchhoff diffraction stack migration
! of common-offset seismic data
!                                      Hocine TABTI, Mars 2001
! Modified:    Thomas HELLMANN, Janvier 2003
!======================================================================
!

IMPLICIT NONE

character(80)     parfile, imgfile, tfile, seisfile, pfile

character         NO, type

integer           seisflag, ampflag, ouver

integer           FBUF(60)     ! Trace header (SEG-Y &  SU)
```

```
integer          nzt, nxt, nst   ! Dimension of traveltime table

integer          nzo, nxo        ! Dimension of output image

real             fzt, dzt, fxt, dxt, fst, dst ! Traveltime param.

real             xo,zo,fzo, dzo, fxo, dxo ! image param.

integer(2)        nt    ! number of samples in input traces

real(8)           dt    ! sampling interval in input traces

real             dx    ! sampling interval of midpoints

real             v0,lst,a1,a2,tmax

integer          enr          ! size (in bytes) of records

integer          i,j,k,l,m,n,imax,jmax,msmooth,ibeg,idt,ixpos,izpos,ispos,irpos,itp

integer          ntrace,m,iiend,iibeg

real             w1,w2,w,tz1,tz2,PI

real(8)           ts,tr

real             a(500),b(500),smooth(60)  ! Amplitude and smooth vect.

integer           xs,xr  ! Source/Receiver coord. on seismic trace

real(8)           matpic(200,200)
```

```
write(*,*)
write(*,*)'        ENTER THE MIGRATION PARAMETERS FILENAME'
write(*,*)'+-------------------------------------------------+'
write(*,*)'| This file contains information needed for migration |'
write(*,*)'| including the travel-time table specifications      |'
write(*,*)'| Together with the time-offset input traces settings |'
write(*,*)'| and the desired output depth-image traces parameters|'
write(*,*)'| See example in log.par                              |'
write(*,*)'+-------------------------------------------------+'
read(*,*)parfile
open(unit=9, file=parfile, form='formatted', status='old')

write(*,*)' Kirchhoff summation type:'
write(*,*)'  f    = Full aperture'
write(*,*)'  s    = Aperture selection'
write(*,*)'  n    = No summation (output log-image)'
read(*,*)type

IF (type == 's') THEN
  write(*,*)' Picks file location:'
  read(*,*)pfile
  write(*,*)' Migration aperture:'
  read(*,*)ouver
ENDIF

! Reading information from parfile
!---------------------------------

! travel-time table filename
```

```
read(9,*)
read(9,*)tfile

! constant-offset seismic data filename
read(9,*)
read(9,*)seisfile

! flag for seismic data format (1=SU format; 2=SEG-Y format)
read(9,*)
read(9,*)seisflag

! Desired output image filename
read(9,*)
read(9,*)imgfile

! first depth sample in traveltime table [m]
read(9,*)
read(9,*)fzt

! number of depth samples in traveltime table
read(9,*)
read(9,*)nzt

! depth interval in traveltime table [m]
read(9,*)
read(9,*)dzt

! first lateral sample in traveltime table [m]
read(9,*)
read(9,*)fxt
```

```
! number of lateral samples in traveltime table
read(9,*)
read(9,*)nxt

! lateral interval in traveltime table [m]
read(9,*)
read(9,*)dxt

! x-coordinate of first source in traveltime table [m]
read(9,*)
read(9,*)fst

! number of sources in traveltime table
read(9,*)
read(9,*)nst

! x-coordinate increment of sources [m]
read(9,*)
read(9,*)dst

! z-coordinate of first point in output trace [m]
read(9,*)
read(9,*)fzo

! vertical sampling of output trace [m]
read(9,*)
read(9,*)dzo

! number of points in output trace
read(9,*)
read(9,*)nzo
```

```
! x-coordinate of first output trace [m]
read(9,*)
read(9,*)fxo

! horizontal spacing of output log-image [m]
read(9,*)
read(9,*)dxo

! total number of input cst offset seismic traces
read(9,*)
read(9,*)ntrace

! number of output traces
read(9,*)
read(9,*)nxo

! reference velocity for amplitude correction
read(9,*)
read(9,*)v0

! flag for amplitude correction (0=none; 1=include)
read(9,*)
read(9,*)ampflag

! HALF Length of the smoothing operator (triangle) [in samples]
! REM: NOT INCLUDING THE CENTRAL SAMPLE i.e. triangle summit
read(9,*)
read(9,*)msmooth

! INITIALISE THE SMOOTHING TRIANGLE FUNCTION
```

```
! ----------------------------------------

smooth=0.0d0
DO i=1,msmooth
  smooth(i)=float(i)/(msmooth+1)
  smooth(2*msmooth-i+2)=smooth(i)
  ENDDO
smooth(msmooth+1)=1.

PI = ATAN(1.0)*4

! read time param. from the input cst offset seismic data
! ------------------------------------------------------

call OPEN (41,seisfile,'old',2)
ibeg=0
IF (seisflag .eq. 2) ibeg=1800
read(41,rec=ibeg+57)nt
read(41,rec=ibeg+58)idt
close(41)

dt=float(idt)/1000

write(*,*)'> Number of samples per trace : ',nt
write(*,*)'> Sampling interval (in msec) : ',dt
write(*,*)'Do you want to reajust the previous parameters (y/n)? [n]: '
read(*,*) NO
IF (NO == 'Y' .OR. NO == 'y') THEN
write(*,*)
write(*,*)'Please give the right values in the '
write(*,*)'same order as they are printed previously.'
```

```
read(*,*)nt,dt
        ENDIF
dt=dt/1000
write(*,*)'Current parameters:'
write(*,*)'Number of samples per trace: ',nt
write(*,*)'Sampling interval: ',dt,'s'
tmax=(nt-1)*dt           ! Maximum time in input seismic traces
ibeg=0

! OPEN INPUT AND OUTPUT FILES
! ---------------------------
call OPEN (41,seisfile,'old',4)
call OPEN (42,tfile,'old',4)
call OPEN (43,imgfile,'new',4)

! INPUT THE PICK TABLE FILE
! -------------------------
IF(type == 's') THEN
open(11,file=pfile,form='formatted',status='old')
write(*,*)'Inputting traveltimes table file'
DO i=1,nzo
  read(11,*)(matpic(i,j),j=1,nxo)
ENDDO
close(11)
ENDIF

IF (seisflag == 2) ibeg=900

! HERE STARTS THE MIGRATION
! -------------------------
lst=(nst-1)*dst+fst   ! Last source/receiver position in traveltime table
```

```
! LOOP ON HORIZONTAL SAMPLES
! --------------------------
DO j=1,nxo
xo=fxo+(j-1)*dxo
write(*,*)
write(*,*)' X-POS',xo,' (->',(nxo-1)*dxo+fxo,')'
ixpos=int((xo-fxt)/dxt)+1

! LOOP ON DEPTH SAMPLES
! ---------------------
DO i=1,nzo-1
zo=fzo+(i-1)*dzo
     izpos=int((zo-fzt)/dzt)+1  ! also used for interpolation below

! LOOP ON SEISMIC TRACES
! ----------------------
a=0.0d0            ! Initialise ampl. to zero
DO 300 k=1,ntrace
       irec=ibeg+(k-1)*(60+nt)
       read(41,rec=irec+19)xs
      read(41,rec=irec+21)xr

! CHECK IF THE SOURCE/RECEIVER POS. BELONGS TO THE T_TABLE DOM.
! ------------------------------------------------------------
IF(xs < fst .or. xs > lst) GOTO 300
IF(xr < fst .or. xr > lst) GOTO 300
       ispos=int((xs-fst)/dst)+1
       irpos=int((xr-fst)/dst)+1

! INTERPOLATION OF THE TRAVELTIME TABLE
```

```
! ------------------------------------
! Only depth interpolation is done here
! ------------------------------------

! READ ........
! ----
irec=(ixpos-1)*nzt+(ispos-1)*nxt*nzt+izpos
read(42,rec=irec)tz1
read(42,rec=irec+1)tz2
IF(tz1 > tmax .or. tz2 > tmax)GOTO 300

! ...... AND INTERPOLATE T_TABLE at source POS.
!        -------------------------------------
w1=zo-(izpos-1)*dzt-fzt            ! Weight factor
w2=abs(zo-izpos*dzt-fzt)           ! Weight factor
IF(w1 /= 0.) THEN
ts=(tz1/w1+tz2/w2)/(1/w1+1/w2)
ELSE
        ts=tz1     ! Traveltime from source to img. point
ENDIF

! DO THE SAME AT the receiver POS.
! --------------------------------
irec=(ixpos-1)*nzt+(irpos-1)*nxt*nzt+izpos
read(42,rec=irec)tz1
read(42,rec=irec+1)tz2
IF(tz1 > tmax .or. tz2 > tmax)GOTO 300
IF(w1 /= 0.) THEN
        tr=(tz1/w1+tz2/w2)/(1/w1+1/w2)
ELSE         ! Traveltime from receiver to img. point
        tr=tz1
```

```
ENDIF
IF(tr+ts > tmax)GOTO 300

! READ TRACE AMPLITUDES AND INTERPOLATE AT time ts+tr
! ---------------------------------------------------
itpos=int((ts+tr)/dt+0.00001)+1
irec=ibeg+(k-1)*(nt+60)+itpos+60
read(41,rec=irec)a1
read(41,rec=irec+1)a2
w1=ts+tr-(itpos-1)*dt           ! Weight factor
w2=abs(ts+tr-itpos*dt)          ! Weight factor
IF(w1 /= 0.) THEN
        a(k+msmooth)=(a1/w1+a2/w2)/(1/w1+1/w2)
ELSE
        a(k+msmooth)=a1             ! Amplitude at time ts+ts
ENDIF

! APPLY AMPLITUDE CORRECTION IF RECQUIRED
! ---------------------------------------
IF(ampflag == 1 .and. ts > 0. .and. tr > 0.) THEN
        w=zo*(ts+tr)**(3/2)*(1/ts**2+1/tr**2)&
        &*sqrt(1-(xs-xr)**2/(v0**2*(ts+tr)**2))
        a(k+msmooth)=a(k+msmooth)*w*sqrt(2/PI)/v0**2
ENDIF

300 CONTINUE          !!! END of Loop on SEISMIC traces

! Smoothing the migration operator for specular-ray select.
! *********************************************************
b=0.0d0
DO l=msmooth+1,k+msmooth-1
```

```
b(l)=SUM(a(l-msmooth:l+msmooth)*smooth(1:2*msmooth+1))
ENDDO

IF(type == 'n') THEN
! Write The result to output log-image file
! ----------------------------------------
DO m=1,k-1
  irec=(m-1)*nzo+(j-1)*nzo*ntrace
  write(43,rec=irec+i)b(m)
ENDDO
ENDIF
IF(type == 'f') THEN
! Write the full-aperture summation to image file
! ---------------------------------------
  irec=(j-1)*(60+nzo)+60
  write(43,rec=irec+i)SUM(b(1:ntrace))
ENDIF
IF(type == 's') THEN
! Write the aperture-selected summation to image file
! ---------------------------------------
  iibeg=abs(matpic(i,j)/25)-ouver
  iiend=abs(matpic(i,j)/25)+ouver
  IF(iibeg < 1)iibeg=1
  IF(iiend > ntrace)iibeg=ntrace
  irec=(j-1)*(nzo+60)+60
  write(43,rec=irec+i)SUM(b(iibeg:iiend))
ENDIF

ENDDO          !!! END of Loop on DEPTH samples

IF(type == 'n') THEN
```

```
! Complement the last sample with 0 value
! ---------------------------------------
  irec=(m-2)*nzo+(j-1)*nzo*ntrace
  write(43,rec=irec+i)0.
ENDIF

IF(type == 's' .or. type == 'f') THEN
! Complement the last sample with 0 value
! ---------------------------------------
  write(43,rec=irec+i)0.
! Write TRACE HEADER to the current image trace
! -------------------------------------------
  FBUF=0           ! Initialise Trace Header to zero
  FBUF(1)=j
  FBUF(2)=j
  FBUF(6)=int(xo)
  FBUF(7)=1
  FBUF(29)=nzo
  irec=(j-1)*(60+nzo)
  DO i=1,60
    write(43,rec=irec+i)FBUF(i)
  ENDDO
ENDIF

ENDDO          !!! END of Loop on HORIZONTAL SAMPLES

write(*,*)' MIGRATION TERMINATED '
write(*,*)' Useful Information '
write(*,*)'ns=',nzo,' dt=',dt,' d1=',dzo,' d2=',dxo
write(*,*)'n2=',nxo,' f1=',fzo,' f2=',fxo
```

```
END PROGRAM



!-------------------------------------------------------------

subroutine OPEN (unt,fle,stat,enr)
       character(80) fle
       character(3) stat
       integer unt
       integer enr
       open(unt,file=fle,access='direct',form='unformatted',&
          &status=stat,recl=enr)
       return
       end
!-------------------------------------------------------------
```

Appendix B

Fresnel aperture picking program

```
clear;

prompt={'Image filename (*.img):','Picks filename (*.pit) (if needed):','Number of
tit='Input for editing';
def={'../tests/simple_model/pck*_smth6.img','../tests/simple_model/pck*.pit','301',
answer=inputdlg(prompt,tit,1,def,'on');
b=cell2struct(answer,{'filename','pickname','ns','nx','dx','dz','dana'},1);
filename=b.filename;
pickname=b.pickname;
ns=str2num(b.ns);
nx=str2num(b.nx);
dx=str2num(b.dx);
dz=str2num(b.dz);
dana=str2num(b.dana);

% open and read the data file
  filein=fopen(filename,'r');
  dat=fread(filein,inf,'real*4');
```

```
  fclose(filein);
% compute usefull variables
  npanel=size(dat)/(nx*ns);
  'The number of panels is: ',npanel(1,1)
% read some computer's parameters
  scrsize=get(0,'ScreenSize');

% import the picks file matrix
  pp=0;
  if pickname~=0
    prevpicks=load(pickname);
    for m=1:npanel(1,1);
      prevpic(:,m)=prevpicks(:,(m-1)*dana/dx+1);
    end;
    pp=1;
    clear prevpicks;
  end;

%%%%%%%%%%%%%%%%%%%%%%%%%%%%%%%%%%%%%%%%%%%%%%%%%%%%%%%%%%%%%%%%%%%%%%%%%%%%
%%%%%%%%%%%%%%%%%%%%%% here starts the processing %%%%%%%%%%%%%%%%%%%%%%
  for m=1:npanel(1,1)

    back=0;
%   create the image matrix
    for i=1:nx;
      for j=1:ns;
        matr(j,i)=dat((nx*ns*(m-1))+j+(ns*(i-1)));
      end;
    end;
%   create the grid
    x=0:dx:dx*nx-1;
```

```
    z=0:-dz:-dz*(ns-1);

%%%%%%%%%%%%%%%%%%%%%%%%%%%%%%%%%%%%%%%%%%%%%%%%%%%%%%%%%%%%%%%%%%%%%%%
%%%%%%%%%%%%%%%%%%%%%% picking process %%%%%%%%%%%%%%%%%%%%%%
%   draw the image and the previous trend
    fg=figure(m);

    set(fg,'Position',[200 200 nx*dx/5 ns*dz/5]);
    set(fg,'Resize','off');
    colormap('jet');
    imagesc(x,-z,abs(matr));
    hold on;
    colorbar;
    if m>1
      plot(inter(:,m-1),-z,'k.');
    end;
    hold on;
    if pp==1
      plot(prevpic(:,m),-z,'r-');
    end;
    hold off;

%   display a message
    messge=[' Press "OK" to start!                                  ';
            ' Press left mouse button to pick!                      ';
            ' Press 2nd mouse button to go to the previous panel!';
            ' Press right mouse button to go to the next panel!  '];
    msgbox(messge,'Info','warn','modal');

    itera=1;
    [testx,testz,msbtn]=ginput(1);
```

```
    while (msbtn~=3)
      [testx,testz,msbtn]=ginput(1);
      if msbtn==1
        pic(itera,1)=testx
        pic(itera,2)=testz
        itera=itera+1;
      end;
      if msbtn==2
        back=1;
        m=m-1;
        break;
      end;
      if pp==0 && itera==1 && msbtn==3
        msg=msgbox(['No pick has been input!'],'Warning!','error','nonmodal');
        pause(2);
        close(msg);
        msbtn=2;
      end;
    end;
    delete(fg);

    if back==0 || itera>1

%%%%%%%%%%%%%%%%%%%%%%%%%%%%%%%%%%%%%%%%%%%%%%%%%%%%%%%%%%%%%%%%%%%%%%%%%%%%%%%%
%%%%%%%%%%%%%%%%%%%% interpolation in depth of the picks %%%%%%%%%%%%%%%%%%%%
%     "extrapolates" the picks coordinates in z=0 and z=ns*dz
      sample(1,1)=(nx/2)*dx;
      sample(1,2)=0;
      for p=1:itera-1;
        sample(p+1,1)=pic(p,1);
        sample(p+1,2)=pic(p,2);
```

```
      end;
      sample=sortrows(sample,2);
      sample(itera+1,1)=sample(itera,1);
      sample(itera+1,2)=ns*(dz);
      xpick=sample(:,1);
      zpick=sample(:,2);

      for l=1:ns;
        inter(l,m)=interp1(zpick,xpick,(l-1)*(dz));
      end;

%     clear some variables
      clear sample;
      clear pic;

%   fin de la condition if
    end;

%   don't modify the previous picks if no new pick
    if itera==1 && pp==1
      inter(:,m)=prevpic(:,m);
    end;

% fin de la boucle for
  end;


% wait for user feedback before interpolating
  choice1=menu('Display the overview of the panels?','Yes','No');
  if choice1==1
%%%%%%%%%%%%%%%%%%%%%%%%%%%%%%%%%%%%%%%%%%%%%%%%%%%%%%%%%%%%%%%%%%%%%%%%%%%
```

```
%%%%%%%%%%%%%%%%% display the panels and picks %%%%%%%%%%%%%%%%%%%%
    axis off;
    ndisp=ceil(npanel(1,1)/12);
    s=1;
    for m=1:ndisp:npanel(1,1)
%     create the image matrix
      for i=1:nx;
        for j=1:ns;
          matr(j,i)=dat((nx*ns*(m-1))+j+(ns*(i-1)));
        end;
      end;
%     draw the image
      figure(99);
      colormap('jet');
      subplot(3,4,s);
      s=s+1;
      imagesc(x,-z,abs(matr));
      hold on;
%     draw the picks and their interpolation
      plot(inter(:,m),-z,'k-');
      hold on;
    end;
  end;
  hold off;
  axis on;

% wait for user feedback before interpolating
  choice2=menu('Interpolated horizontally the picks table?','Yes','No');
  if choice2==1
%%%%%%%%%%%%%%%%%%%%%%%%%%%%%%%%%%%%%%%%%%%%%%%%%%%%%%%%%%%%%%%%%%%%%%%%%%%%%%%
%%%%%%%%%%%%%%%%%%%%%% interpolation in x of the picks %%%%%%%%%%%%%%%%%%%%%%
```

```
    coorana=0:dana:(npanel(1,1)-1)*dana;
    for q=1:ns;
      for r=1:(npanel(1,1)-1)*dana/dx+1;
        pictable(q,r)=interp1(coorana,inter(q,:),(r-1)*dx,'spline');
      end;
    end;

%   plot the interpolated curve for each horizontal sample
    figure(m+1);
    set(m+1,'Position',[200,200,nx*dx/5,ns*dz/5]);
    set(m+1,'Resize','off');
    for s=1:(npanel(1,1)-1)*dana/dx+1;
      axis([0 6000 -5000 0]);
      plot(pictable(:,s),z,'k:');
      hold on;
    end;
    hold off;
  end;

% output the interpolated picks matrix in a file
  choice3=menu('Output picks table to file?','Yes','No');
  if choice3==1
    save pick.pit pictable -ascii;
  end;

  close all;
```

Appendix C

Article from First Break

Fresnel aperture prestack depth migration

Hocine Tabti*, Leiv-J. Gelius, and Thomas Hellmann****

Abstract

We investigate possible improvements in seismic imaging. We discuss how the Fresnel zone relates to the migration aperture and introduce the concept of the Fresnel aperture, which is the direct time-domain equivalent, at the receivers' surface, of the subsurface Fresnel zone. Through these concepts we propose a new and efficient method for optimal aperture selection and migration. For complex media, multipathing will occur and multiple Fresnel apertures can exist for a given image point. In practice, due to inaccuracies and smoothing of the background velocity macromodel, inaccuracies in the ray-tracing method used for Green's function computations and possible noise corruption of the data, the true Fresnel apertures will, in many cases, be replaced by 'false' ones, with apparently new Fresnel apertures being added. Hence, contributions from these 'false' Fresnel apertures cause a noise-corrupted image of the subsurface. It is now assumed that the single-scattered events are quite robust with respect to the above-mentioned distortions, and that their corresponding Fresnel apertures will remain essentially undistorted, with the strongest amplitudes. Based on this main assumption, we propose a method, analogous with velocity analysis, where the strong-amplitude Fresnel apertures can be picked interactively and at least semi-automatically. However, as in velocity analysis, a certain amount of user interaction has to be assumed. When this technique is combined with a prestack Kirchhoff-type depth-migration method, we call it Fresnel-aperture PSDM. This imaging method has been applied to data from both the Marmousi model and the North Sea. In both cases the improvements, when compared to conventional imaging, were considerable.

Introduction

Improving the resolution of seismic images is one of the most challenging topics in geophysics. In the study presented here, we investigate the consequences of the band-limited nature of seismic data when forming images of the subsurface. We propose a new and efficient method for the so-called specular-ray selection which we denote Fresnel-aperture selection. Previous work based on the so-called projected Fresnel zone (Schleicher *et al.* 1997; Vanelle & Gajewski 2001) reported an improvement in the S/N ratio only for data of rather poor quality. Moreover, these works imply some knowledge of the reflectors, including computation of curvature information, which can be both cumbersome and difficult in complicated media. Other authors (Tygel *et al.* 1993) used the so-called multiple-weights diffraction stack. This method, based on the work of Bleistein (1987), selects only the specular source–receiver pairs, leaving the estimation of the Fresnel aperture size to the user.

The method presented here does not require any knowledge apart from the conventional traveltime table and includes geometry and nature of all the scattering objects (i.e. reflectors and diffractors). It is also perfectly stable whatever the complexity of the medium under consideration. In the case of an accurate and simple velocity model, high-quality data and a negligible multiple-contribution conventional Kirchhoff diffraction stack, employing the complete data set gives very much the same result as our optimized aperture selection. However, for complex models and noise-contaminated data, we demonstrate the possibility of significantly improving the image quality with the help of the Fresnel aperture concept underlying the specular-ray selection. Note that, if a wavefront-orientated ray-tracing method is being used (Coman & Gajewski 2002), multivalued traveltime tables can be computed with great accuracy but this is still time-consuming. However, we believe that in general cases involving complex media, multipathing imaging is not an easy task, due to imprecisions in the velocity macromodel, inaccuracies in the ray tracing and the problem with noisy data including possible multiples. Furthermore, in multipathing imaging, the entire multichannel data set must be processed at one time (Operto *et al.* 2000), and applications to individual common-offset gathers may provide spurious artefacts in the individual migrated images (Xu *et al.* 1998). This phenomenon can be explained in our terminology by the so-called 'false' Fresnel apertures.

Specular rays and Fresnel zones

In the high-frequency limit, the approximate solution to the wave equation is described by ray theory. The high-frequency condition is in fact equivalent to assuming that the velocity within the medium of propagation is piecewise smooth compared to the wavelength of the source pulse. Local discontinuities between continuous blocks or layers can be handled kinematically by the reflection/transmission conditions. The trajectory of the wave energy between a given source–receiver pair is then described by geometrical optics obeying Fermat's principle of stationarity, which also governs the reflection/transmission paths or the so-called specu-

** Formerly University of Oslo, Department of Geology, Blindern, Oslo; presently PGS Geophysical AS, Strandveien 4, P.O.Box 290, N-1326, Lysaker, Norway. E-mail: Hocine.Tabti@pgs.com*

*** University of Oslo, Department of Geology, P.O.Box 1047 Blindern, N-0316, Oslo, Norway.*

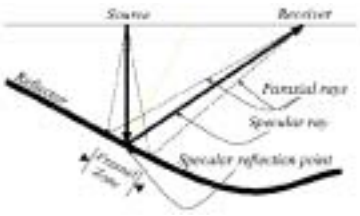

Figure 1 *Illustration of the specular ray and the Fresnel zone in a single reflection experiment.*

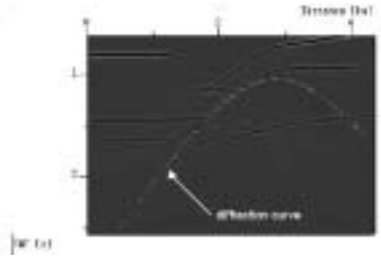

Figure 2 *The time-diffraction curve corresponding to point A (see Fig. 3) superimposed on the zero-offset seismic section calculated from the velocity model in Fig. 3.*

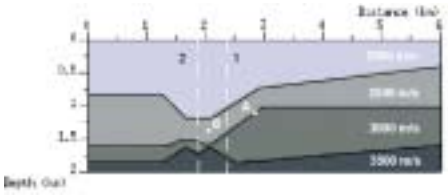

Figure 3 *The velocity model used in the modelling of the zero-offset data and the calculation of the traveltime table (i.e. the time-diffraction curves). The figure also indicates the positions of the points A and B and the vertical profiles 1 and 2 investigated in this paper.*

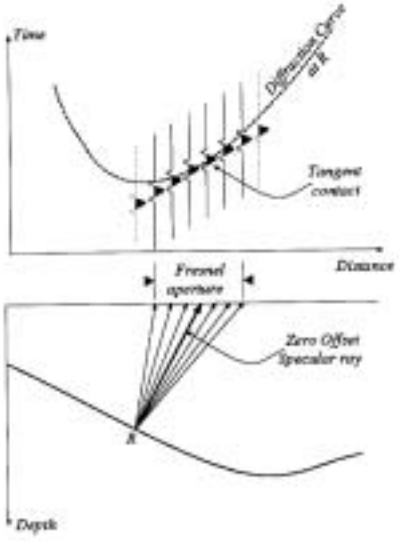

Figure 4 *Illustration of the Fresnel aperture for a zero-offset reflection experiment. The time-diffraction curve corresponding to reflection point R is 'tangential' to the zero-offset seismic events and passes through non-negligible amplitudes within the Fresnel-aperture segment.*

lar rays. Similarly, we shall call the impact of the specular rays on the reflectors the 'specular reflection points' (Fig. 1). Note that the other 'paraxial' rays surrounding the specular ray in Fig. 1 (also in Fig. 4) do not obey Fermat's principle and will therefore not be predicted by geometrical ray tracing as is the case for the specular ray.

In the theoretical limit of infinite bandwidth, the specular rays describe the phenomenon exactly. However, in practice we deal with band-limited pulses, which is particularly important when the velocity macromodel includes sharp discontinuities such as reflectors, edge diffractors and other scattering objects. These sharp variations cannot accommodate the relatively low frequencies of the actual pulse when classical ray theory is used. A well-known fact is that the reflection/transmission of the incident seismic pulse involves an appreciable volume around the specular reflection point rather than just the point itself as described by geometrical optics rays (Hubral *et al.* 1993). As waveforms are really non-planar, reflections from a surface are returned from a region and over an interval of time. Signal that is received at approximately the same time cannot be separated into individual components. Thus, we see that reflections that can be considered as almost coincident in time at the receiver come from a region (see Fig. 1). The area that produces the reflection is known as the first Fresnel zone (Sheriff 2002). For a coincident source and receiver, this zone is circular and is defined by the family of paraxial rays with a phase difference relative to the central (specular) ray of less than half a (dominant) wavelength. If the (dominant) wavelength of the pulse is large then the zone from which the reflected energy returns is larger and the resolution is lower. Note that the concept of a Fresnel zone (or zones) was originally defined in optics for pure harmonic waves (Sheriff 1980; Knapp 1991). Finally, it is worth observing that it is, nonetheless, possible to use the ray theory with some additional effort (dynamic ray tracing) to estimate the Fresnel region around a given specular ray trajectory (Červený & Soares 1992).

Kirchhoff PSDM and specular-ray selection

In the work presented here, we employ a prestack Kirchhoff depth migration algorithm to study the so-called specular-ray selection. By the term specular-ray selection, we mean selecting that part of the data which gives a constructive response, and only using this data in the migration sum. This technique will be discussed in detail in later paragraphs. The theory of Kirchhoff migration itself has been widely developed in the literature and so we will limit our discussion to the elements directly related to the present work.

For the sake of clarity we now give a brief explanation of the Kirchhoff diffraction-stack technique in practice. For simplicity we omit the weighting and filtering of the data, which can be safely ignored in the present study. Figure 2 shows a synthetic 2D acoustic zero-offset section calculated from the velocity model shown in Fig. 3. The time-diffraction curve corresponding to point *A* is superimposed on the zero-offset

seismic traces. This time-diffraction curve corresponds to what we will measure *kinematically* at the surface with a zero-offset configuration (i.e. coincident sources and receivers), if the subsurface model consists of a scatterer at point *A*. All the seismic energy lying along this diffraction curve is summed to form the amplitude at the image point *A*. When the same operation is repeated for all the image points we obtain the migrated or image section. Note that although the discussion in the present work involves only 2D examples, this is done for the sake of simplicity. All the arguments and conclusions reached are also valid for the general 3D case. We need only to replace lines by surfaces and sections by volumes or cubes.

The Fresnel aperture

Since the image point *A* in Fig. 3 is located on a reflector, its diffraction curve (see Fig. 2) is 'tangential' to the zero-offset reflected energy in a region surrounding the point of emergence of the corresponding specular reflection ray at the receiving array (see Fig. 4). (Note that the term 'tangential' is used here to describe a zone of contact rather than a point, due to the low band of source frequencies.) This is a general observation and occurs in all cases involving an image point located on a reflecting or diffracting surface. We denote this tangential contact the *Fresnel aperture* due to its close relationship to the Fresnel zone. In fact, the correspondence between the Fresnel zone and the Fresnel aperture is precisely the link required to relate the time-domain seismic energy to the space-domain image of the subsurface scattering objects. As stated by Sheriff & Geldart (1995, p.155): 'a specific portion (or point) of the reflector will contribute to all of the seismic traces whose Fresnel zones include the portion (or the point)'. The envelope of the cluster of seismic traces thus contributing to the image of a common point on the reflector forms what we call here the Fresnel aperture. The term contribute implies that the Fresnel zone of each trace includes the image point considered. We disagree with Schleicher *et al.* (1997) and Hubral *et al.* (1993) who equate the Fresnel aperture with the projected Fresnel zone of the actual reflection. This equivalence is justified only if the Fresnel zones of all the reflections within the actual Fresnel zone have the same dimensions. A homogeneous medium involving a flat reflecting surface is an example of such a case. However, in arbitrary heterogeneous media, the sizes of the Fresnel zone and the Fresnel aperture are generally different for band-limited signals.

The Fresnel aperture shrinks as the frequency content of the source pulse broadens to include higher frequencies. In the limit of a perfect impulse response, the tangential contact reduces to a single point that corresponds to the specular ray (see Fig. 4) (Schleicher *et al.* 1993). Note that a perfect diffraction point is an exception to the previous rule. In that case, the corresponding diffraction curve follows exactly the corresponding scattered seismic events whatever the frequency content of the source pulse, and the Fresnel aperture then extends theoretically to infinity. As will be demonstrated below, one of the advantages of the method of specular-ray selection proposed here is that it includes all possible classes of scattering points. Another important feature is that outside the Fresnel aperture the diffraction curve has short bursts of energy only (see Fig. 2).

Figure 5 shows the same type of computations as in Fig. 2, but for image point *B* (see Fig. 3). Because *B* is not a scattering point there is no tangential contact between its time-diffraction curve and the scattered events of the zero-offset seismic traces. Only the short bursts of energy exist, caused by the occasional passage through the scattered events. As will be shown in the next paragraph, the observations following from Figs 2 and 5 form the basis of our method of specular-ray selection.

Specular-ray and Fresnel aperture selection

We are now in a position to explain what is meant by the specular-ray selection in migration. A perfect migration process is one that collapses and back-propagates the seismic events to their originating scattering (reflecting and diffracting) points. The aim of the specular-ray selection in migration is to collect only the events that actually originated (i.e. were scattered) from the portion of the reflector we want to image. Hence, only events within the Fresnel aperture will contribute *constructively* to the sum along the time-diffraction curve. Therefore, an efficient specular-ray selection in migration must not only contain the specular event itself but also the relevant area surrounding it, i.e. all the events within the Fresnel

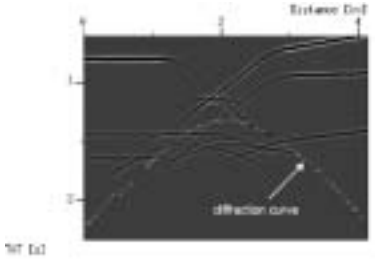

Figure 5 *The time-diffraction curve corresponding to point B (see Fig. 3) superimposed on the zero-offset seismic section calculated from the velocity model in Fig. 3.*

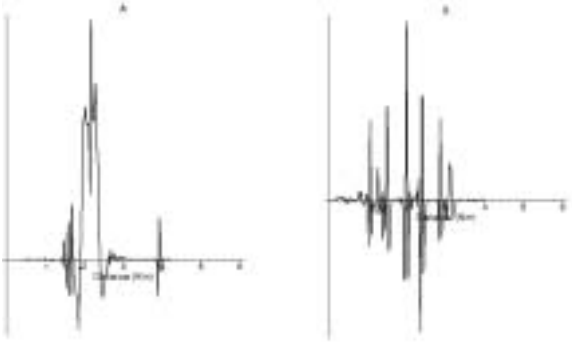

Figure 6 *Amplitudes of the seismic events collected along the time-diffraction curves of (a) point A and (b) point B. These curves are denoted diffraction operators.*

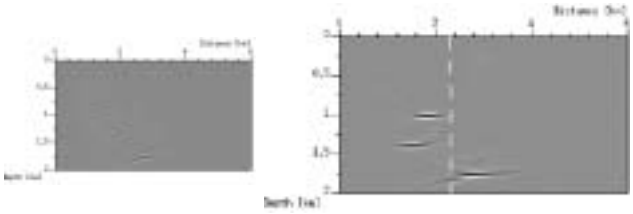

Figure 7 (a) *Raw diffraction-operator panel corresponding to profile 1 (see Fig. 3). (b) The same diffraction operators after low-pass filtering. The vertical dashed white line indicates the position of profile 1.*

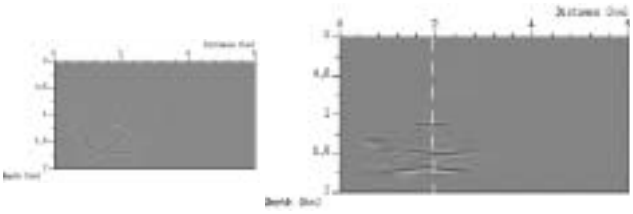

Figure 8 *(a) Raw diffraction-operator panel corresponding to profile 2 (see Fig. 3). (b) The same diffraction operators after low-pass filtering. The vertical dashed white line indicates the position of profile 2.*

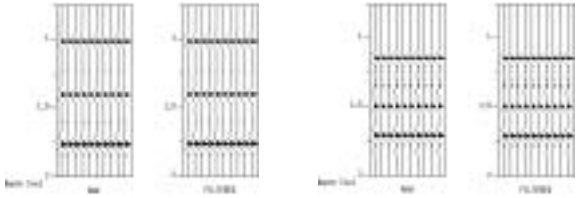

Figure 9 *Image traces corresponding to profile 1 (a) and profile 2 (b) obtained using both the raw diffraction operators (left column) and the low-pass filtered diffraction operators (right column).*

aperture. To avoid confusion, we will, in the following, use the term Fresnel aperture selection instead of specular-ray selection.

Figures 6(a) and (b) represent the amplitudes of the seismic events collected along the time-diffraction curves of points *A* and *B*, respectively. The horizontal abscissa in each figure is simply the *x*-position of the receivers. We denote this type of curve: a diffraction operator. In migration, at each subsurface position, the corresponding *diffraction operator* is summed to form the amplitude at that location.

We can readily see the differences in the amplitude character between the two points. Point *A*, which is located on a reflector (implying a tangential contact between its time-diffraction curve and the seismic events) exhibits a 'low-frequency' amplitude behaviour precisely at the Fresnel aperture location (approximately between 1.8 and 2.4 km). The two passages through the time-diffraction curve, one to the right and the other immediately to the left (see Fig. 2), appear as 'high-frequency' amplitude peaks. In contrast, point *B*, which is not located on a reflector, exhibits only the 'high-frequency' amplitude peaks of the passages through the time-diffraction curve. It is important to realize that these observations are general and that the systematic behaviour shown here *always appears when dealing with band-limited seismic data.*

Our method of Fresnel aperture selection exploits this fact: before we sum up the amplitudes, we first low-pass filter (zero-phase type) the amplitudes extracted along the diffraction curve (i.e. the diffraction operator) to remove or strongly attenuate the high-frequency amplitude peaks thus leaving only the relevant low-frequency part (i.e. the Fresnel aperture area). Secondly, we carry out a spatial selection adding only amplitudes along that 'low-frequency' part of the diffraction curve. Hence, our method of Fresnel-aperture selection consists of two steps: low-pass filtering and muting. In the remaining part of this section we consider only the low-pass filtering step and compare migrated data with and without this filtering. The spatial-selection step will be discussed in later paragraphs.

In Fig. 7(a), we plot, employing a seismic plotting style, the diffraction operators corresponding to a vertical profile at the horizontal position indicated by #1 in Fig. 3. This plot is constructed from diffraction operators of image points sampled at intervals of 10 m along the profile. If, for instance, we plot the amplitudes along a horizontal slice (constant-depth point) in Fig. 7(a), we obtain the diffraction operator corresponding to that subsurface location (i.e. similar to the curves shown in Fig. 6). Figure 7(b) represents the corresponding low-pass filtered version of Fig. 7(a). The vertical dashed white line gives the position of the corresponding profile. From Fig. 3, it follows that this profile cuts reflectors at three different depths, each reflector having a different dip. Therefore we expect that the low-pass filtering identifies three areas (or line segments for a 2D geometry). Depending on the local dip of the corresponding reflector, the Fresnel aperture segments will be offset from the profile position either to the left or to the right. The amount of offset will, in general, depend on the dip, the depth to the reflector and the complexity of the overburden model.

Note the complicated pattern in the unfiltered diffraction-operator panel (see Fig. 7a) despite the fairly simple velocity model. This is due to conflicting dips along the profile combined with the proximity of diffracting structures as can be seen from Fig. 3. The corresponding filtered panel (Fig. 7b) shows clearly the efficiency of our method in selecting not only the specular rays but all the corresponding Fresnel apertures. The depths of the selected Fresnel apertures correspond exactly to the depths of the corresponding reflectors (compare Figs 3 and 7b). Moreover, the horizontal positions of the Fresnel aperture segments relative to the profile position reflect the corresponding reflectors' dips. The two first reflectors cut by profile 1 dip to the left and hence the positions of the corresponding Fresnel apertures are shifted to the left relative the vertical position line. Similarly, the Fresnel aperture of the third reflector is offset to the right since it corresponds to a right-dipping reflector. Note, however, in the case of a *complex* overburden the correspondence between a reflector's

dip and its position in the diffraction-operator panel will be more complicated.

So far we have considered only reflected contributions and therefore we now give an example involving diffracting structures in order to demonstrate the efficiency of our method in such a case. To this end we chose a profile passing through a reflector and through, or very close to, two diffracting edges in the model shown in Fig. 3 (#2). The raw diffraction operators and their corresponding low-pass filtered versions are shown in Figs 8(a) and (b), respectively. Consider now the deepest diffracting edge that corresponds to the deepest Fresnel aperture in Fig. 8(b). Since the diffracted energy contains non-negligible energy only within a limited zone, the corresponding Fresnel aperture is also limited, depending on the diffraction amplitudes. However, we can see that the extension is larger than for a pure reflection point (cf. the shallowest Fresnel aperture in Fig. 8b). The geometry of the edge (almost symmetrical for this profile) is responsible for the (almost) centred position of the corresponding Fresnel aperture with respect to the vertical position line. This is also consistent with the physics of diffractions.

As noted above, the migrated trace at any profile position is obtained simply by *stacking all the traces within the diffraction-operator panel*. Thus by comparing migrated traces obtained from the raw diffraction-operator panel with those computed from the filtered panel, we can identify possible differences. The results of stacking the panels (i.e. both raw and filtered versions) of the two profiles considered are shown in Figs 9(a) and (b). Each image trace is plotted 10 times to make the comparison easier. There are hardly any visible differences (either in relative amplitudes or in phase) between the image traces obtained after the low-pass filtering (i.e. stack of the filtered panels) and those obtained by the normal migration process (i.e. stack of raw panels). The same conclusion is obtained if we consider more complex models. Figure 10 shows a constant-offset Kirchhoff prestack depth migration (PSDM) image of a selected deep part of the complex Marmousi model (the target area is shown in Fig. 12 and is discussed in more detail in later sections). The migration is based on near-offset data (200 m) and the complete data aperture. Correspondingly, Fig. 11 shows the result obtained if the diffraction-operator panels are low-pass filtered before Kirchhoff summation. Once again, there are no noticeable differences between the two images.

This main result is, however, not surprising. In the high-frequency limit, the asymptotic version of the migration operator predicts a non-negligible contribution only from the source–receiver pairs belonging to the so-called stationary points. These points are precisely those connecting the source–receiver pairs to the specular reflection points (see e.g. Bleistein 1987). We have seen that the concept of specular rays and specular reflection points in the high-frequency limit extends to the concept of Fresnel apertures and Fresnel zones in the band- limited case. Similarly, the solution of the migration operator extends, in the band-limited case, to include the constructive contribution of the Fresnel aperture, instead of the 'specular source–receiver' contribution only, as in the high-frequency limit. This consistency with the theory of migration is further evidence of the effectiveness of our method of Fresnel aperture selection.

Aperture selection and complex media

We have already seen that the low-pass filtering associated with our Fresnel aperture selection is inherent in the migration process. For ideal data conditions and a simple geological model such as that shown in Fig. 3, we have also seen that no more than one Fresnel aperture exists for a given depth level (in a diffraction-operator panel). However, in cases involving complex media and imperfect data, the concept of Fresnel aperture is of more fundamental interest. It can be used to investigate the cause of artefacts and inaccuracies observed in the migrated image of complex media, since apparently more than one Fresnel aperture can exist at a given depth level in a diffraction-operator panel. Hence, we need to develop a strategy for the second step of our Fresnel aperture procedure, namely the spatial selection, which can be applied in cases of

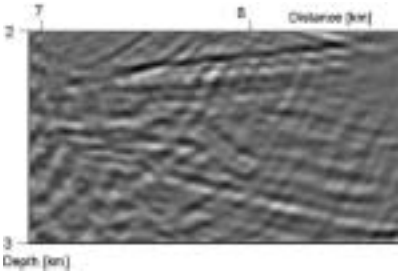

Figure 10 *Constant-offset migration of a deep part of the Marmousi model (target area shown in Fig. 12). Full data aperture and no filtering applied.*

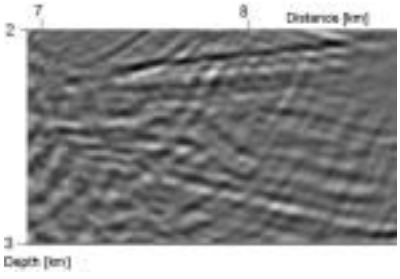

Figure 11 *Constant-offset migration of the same area as in Fig. 10. The result obtained if the diffraction-operator panels are low-pass filtered before Kirchhoff summation (NB. full data aperture).*

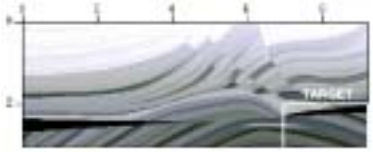

Figure 12 *The Marmousi velocity model with target area.*

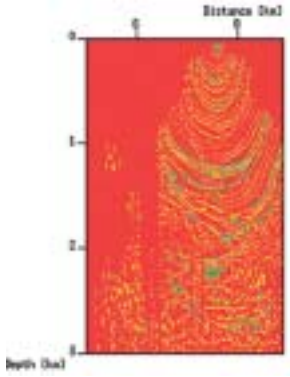

Figure 13 *Raw diffraction-operator panel corresponding to a vertical profile at the horizontal position of 7.6 km in the Marmousi model (see Fig. 12).*

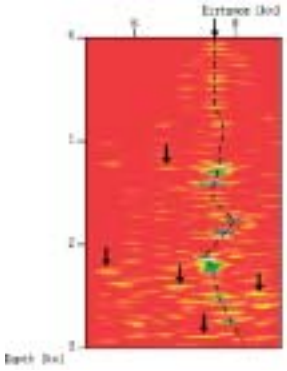

Figure 14 *As Fig. 13 but after low-pass filtering. The black arrow at the top indicates the position of the profile. The dashed line indicates the correct trend to stack around (corresponding to real reflection/diffraction events along the profile). The arrows inside the panel indicate some unwanted events (i.e. ghost reflections) along the profile.*

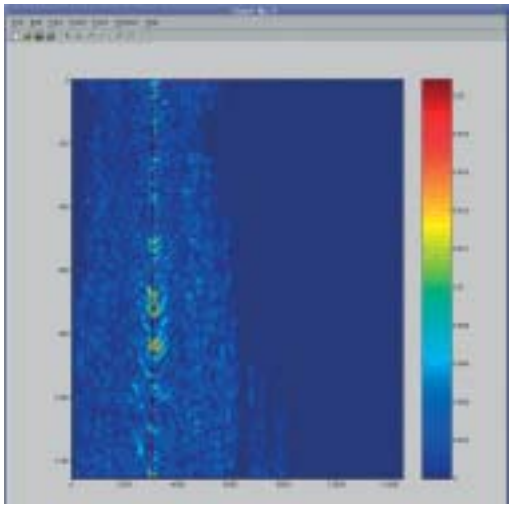

Figure 15 *Example of output from an interactive analysis of a diffraction-operator panel (North Sea data) with the picked stacking trend indicated by the red curve. The picking criterion is based on maximum-amplitude detection.*

conflicting Fresnel apertures.

We now consider Fig. 12 which shows the Marmousi velocity model describing quite complex geological structures. A raw diffraction-operator panel has been computed for constant-offset data (near-offset of 200 m) along the vertical line corresponding to a horizontal position of 7.6 km in this model. The result obtained is shown in Fig. 13 and stacking of this panel gives the image trace at this horizontal location. This panel exhibits a very complicated pattern and is not easy to interpret. Employing the first step of our method of Fresnel aperture selection (i.e. low-pass filtering of Fig. 13), we arrive at the result shown in Fig. 14, which gives a much better insight. When comparing Fig. 14 with Figs 7(b) and 8(b) we see that we no longer have the case of a single Fresnel aperture at a given depth level (i.e. along a horizontal slice). For a certain depth we now observe several apertures, especially for the deeper parts of the panel. Hence, all these apertures contribute constructively to the image point sum. In the migration carried out here, we employed a smoothed version of the Marmousi velocity model and restricted ourselves to singly-scattered Green's functions (employing dynamic ray tracing). There are several causes of these multiple Fresnel apertures, among them being inaccuracies in the traveltime computations and the use of a single wavepath for each subsurface position. Consequently, if the full data aperture is employed in such cases, the migrated image will be contaminated by noise. This type of noise is well known and has been studied in the literature (Geoltrain & Brac 1993; Audebert *et al.* 1997).

Note, however, that for a complex model, *multipathing* can take place and, in the case of triplication, three true Fresnel apertures may exist for the same depth level in a diffraction-operator panel (at least if the full data volume is considered). In practice, due to inaccuracies in the complex velocity model (as well as the smoothing applied), the difficulties of accounting accurately for multipathing, the frequent use of subsets of the data (e.g. constant-offset data) and imperfections such as multiples in the data, we believe that only one Fresnel aperture should be used for each depth level. In order to select the one aperture to be used in the case that several exist, we employ the pragmatic approach of picking the *strongest*. Using this criterion for picking makes it possible to estimate the stacking trend (i.e. the 'centre points' of the true Fresnel apertures). An example of the output from an interactive picking of such stacking trends is shown in Fig. 15, where the diffraction-operator panel is computed from a North Sea data set that will be discussed in more detail below. The red curve represents the picked trend, whereas the superimposed black broken curve represents the trend picked at the previous location of the analysis. The picking of such trend curves has a strong resemblance to velocity picking, and general methods for automatic and interactive picking are adapted from the latter. Finally, sizes of the Fresnel apertures have to be assigned to the aperture curve. The method described here can handle Fresnel aperture variations both within a single image trace and from image trace to image trace. When this tech-

nique is used in combination with prestack Kirchhoff depth migration, we denote it *Fresnel aperture prestack depth migration* (FAPDM).

Data application

In this section, we demonstrate the potential of the FAPDM method employing both synthetic and field data. First we consider the familiar Marmousi model shown in Fig. 12.

Synthetic seismic data exist for this model generated using the acoustic finite-difference technique. In the tests carried out here we chose the target area shown in Fig. 12. First, we carried out the Fresnel aperture analysis as described in the previous paragraph. This analysis was performed every 250 m (23 analyses in total), with spatial interpolation in between. Since we want to study the seismic response as a function of offset (or scattering angle), we consider one offset only (the near-offset of 200 m) to demonstrate the potential of the method. The location of each constant-offset source–receiver pair is then defined by its midpoint, which will now be the horizontal coordinate in the diffraction operator panel. Figure 10 shows the constant-offset migrated image when using the *complete aperture* for each time-diffraction curve. Note that our main interest is in the layers dipping to the right, which include the right-side closure of the reservoir and the oil–water contact (see arrow). The image in Fig. 10 does not resolve these features very well. Figure 16 shows the migrated image obtained employing the Fresnel apertures described above. When comparing this figure with Fig. 10, we can see the improvements for all parts of the target area (compare also with the velocity model in Fig. 12). The overall conclusion is that our FAPDM method works satisfactorily. As a reference, in Fig. 17 we have also computed the FK-filtered version of the migrated image in Fig. 10. When we compare this image with Fig. 16, we find that it lacks both horizontal and vertical resolution.

In the next example we consider a North Sea field data set and chose a target zone involving layers truncated towards the flank of a salt dome. The seismic data were sampled at 4 ms and the record length is 7 s. It is a 60-fold data set with offsets ranging from 108 m to 3083 m. In the migration presented here, we consider only one offset, i.e. the middle-range offset of 1533 m. Velocity analysis was carried out every 2 km for the full data set. Based on these stacking velocities, we computed interval velocities, converted from time to depth and applied smoothing. This smoothed velocity field was then used in the Kirchhoff prestack depth migration. The quality of the velocities for the zone of interest was controlled using image point gathers. Figure 18 shows the migrated image obtained when the complete data aperture is used. The depth range covered by the image is between 1.7 and 3 km, and the horizontal distance is 5 km. We can see from Fig. 18 that the image is corrupted by the same type of passage through linear noise as in the previous example.

We then applied our Fresnel aperture technique to the same zone of interest. The analysis was carried out every 250

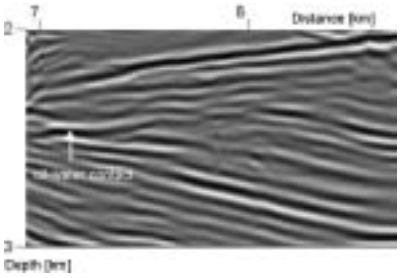

Figure 16 *Constant-offset migration employing the concept of Fresnel aperture selection as described in the text. Selected part of Marmousi model as shown in Fig. 12. Compare with Fig.10.*

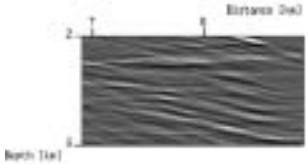

Figure 17 *FK-filtered version of the image in Fig. 10. Note the lack of resolution, both laterally and vertically.*

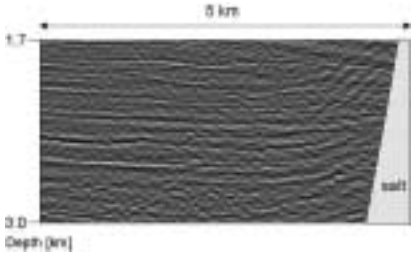

Figure 18 *Full aperture Kirchhoff PSDM of North Sea field data (one offset of 1533 m only).*

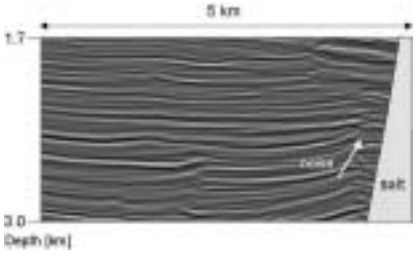

Figure 19 *Fresnel aperture Kirchhoff PSDM of the same data set as shown in Fig. 18. Automatic picking of stacking trends based on maximum-amplitude detection.*

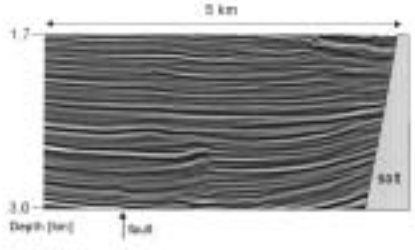

Figure 20 *Fresnel aperture Kirchhoff PSDM of the same data set as shown in Fig. 18. User-guided picking of stacking trends.*

m, with a total of 21 panels to be picked (with spatial interpolation in between). Figure 19 shows the final result obtained using the FAPDM method. Compared to Fig. 18, the image is much better resolved for all parts except close to its right boundary (i.e. where the layers are truncated), where strong ringing events appear. This result is an example of what can happen if only the strongest amplitudes in the diffraction-operator panels are picked. The ringing appearance in Fig. 19 is caused by strong coherent low-frequency noise almost masking the real seismic signals close to the flank of the salt dome. Repeating the Fresnel aperture analysis and picking another trend in the panels close to the flank gives the result shown in Fig. 20. This time the image also resolves the truncated part of the layers very well, and the overall improvement in resolution is striking when compared to Fig. 18. Note for example the small fault system that is marked with the black arrow. However, the overall conclusion is that, just as in the velocity analysis, the Fresnel aperture analysis needs a certain amount of user interaction to ensure an optimal result.

Concluding remarks

The conventional way of performing Kirchhoff (or diffraction-stack) migration is to sum amplitudes collected along diffraction curves (or surfaces in 3D) after optional filtering and weighting. However, we know that the information-carrying trace amplitudes are contained only within a *limited* portion of the diffraction curve. Therefore, adding the amplitudes within that zone would be better than employing the complete aperture if we are dealing with complex media, imperfect data/velocity models and inaccurate traveltime calculations. The problem is then how to select this zone, which we have chosen to denote the *Fresnel aperture* since it is closely linked to the classical Fresnel zone. We have proposed a method for determining these Fresnel apertures, which is based on low-pass filtering of the diffraction-stack operators (i.e. trace amplitude distribution along time-diffraction curves) corresponding to a given image point. In these computations we only need access to the traveltime table. Moreover, our method can handle both reflection and diffraction events. By analogy with velocity analysis, the Fresnel apertures are picked interactively and at least semi-automatically, based on a strongest-amplitude criterion. But as in velocity analysis, a certain amount of user interaction is needed. The corresponding migration method is denoted Fresnel aperture prestack depth migration (FAPDM). It has been applied to data from both the Marmousi model and the North Sea. In both cases the improvements, when compared to conventional Kirchhoff-type PSDM, were considerable.

Acknowledgements

This work was funded by the Research Council of Norway (NFR) through contract 128440/43 ('Improving Prestack Depth Migration by using Resolution Function'). Most of the figures in this paper were obtained using the Seismic Unix (SU) plotting facilities. We thank CGG, Norway, for making the North Sea data set available to us, and IFP (Institut Français du Petrole) for providing the Marmousi data. We also thank Dr. Isabelle Lecomte, NORSAR, for many interesting discussions through the course of this project. Finally, the authors are grateful to Associate Editor Paul Williamson and one anonymous reviewer for many constructive comments and suggestions.

References

Audebert, F., Nichols, D., Rekdal, T., Biondi, B., Lumley, D.E. and Urdaneta, H. [1997] Imaging complex geologic structure with single-arrival Kirchhoff prestack depth migration. *Geophysics* **62**, 1533–1543.

Bleistein, N. [1987] On the imaging of reflectors in the earth. *Geophysics* **52**, 931–942.

Červený, V. and Soares, J.E.P. [1992] Fresnel volume ray tracing. *Geophysics* **57**, 902–915.

Coman, R. and Gajewski, D. [2002] Wavefront-oriented ray tracing with optimal ray density. 64th EAGE conference, Florence, Italy, *Extended Abstracts*, C020.

Geoltrain, S. and Brac, J. [1993] Can we image complex structures with first-arrival traveltime? *Geophysics* **58**, 564–575.

Hubral, P., Schleicher, J., Tygel, M. and Hanitzsch, C. [1993] Determination of Fresnel zones from traveltime measurements. *Geophysics* **58**, 703–712.

Knapp, R.W. [1991] Fresnel zones in the light of broadband data. *Geophysics* **56**, 354–359.

Operto, M.S., Xu, S. and Lambare, G. [2000] Can we quantitatively image complex structures with rays? *Geophysics* **65**, 1223–1238.

Schleicher, J., Hubral, P., Tygel, M. and Jaya, M.S. [1997] Minimum apertures and Fresnel zones in migration and demigration. *Geophysics* **62**, 183–194.

Schleicher, J., Tygel, M. and Hubral, P. [1993] 3-D true amplitude finite-offset migration. *Geophysics* **58**, 1112–1126.

Sheriff, R.E. [1980] Nomogram for Fresnel-zone calculation (Short Note). *Geophysics* **45**, 968–972.

Sheriff, R.E. [2002] *Encyclopedic Dictionary of Applied Geophysics* (4th edition). Society of Exploration Geophysicists.

Sheriff, R.E. and Geldart, L.P. [1995] *Exploration Seismology* (2nd edition). Cambridge University Press.

Tygel, M., Schleicher, J., Hubral, P. and Hanitzsch, C. [1993] Multiple weights in diffraction stack migration. *Geophysics* **59**, 1820–1830.

Vanelle, C. and Gajewski, D. [2001] Determining the optimum migration aperture from travel times. 63rd EAGE conference, Amsterdam, The Netherlands, *Extended Abstracts* A-028.

Xu, S., Chauris, H., Lambare, G. and Noble, M. [1998] Common angle image gather: A new strategy for imaging complex media. 68th SEG meeting, New Orleans, USA, *Expanded Abstracts,* 1704–1707.